



**Y. Shi¹, O. Evtushevsky², G. Milinevsky^{1, 2, 3, *}, A. Grytsai²,
A. Klekociuk^{4, 5}, O. Ivaniha^{2, 3}, Yu. Andrienko²**

¹ International Center of Future Science, College of Physics, Jilin University, Changchun, 130012, China

² Taras Shevchenko National University of Kyiv, Kyiv, 01601, Ukraine

³ State Institution National Antarctic Scientific Center, Ministry of Education
and Science of Ukraine, Kyiv, 01601, Ukraine

⁴ Antarctic Climate Program, Australian Antarctic Division, Kingston, 7050, Australia

⁵ University of Adelaide, Adelaide, 5005, Australia

* Corresponding author: gennadi.milinevsky@knu.ua

The data processing and analysis methods for stratospheric ozone and planetary wave study

Abstract. We describe the methods and data sources for investigating the stratospheric ozone and planetary waves in the atmosphere in the framework of research provided by our international team. Selected ground-based and satellite instruments for ozone measurements and related reanalyses are described. Examples of data and analysis tools are shown. The technique of planetary wave spectral analysis under conditions of dynamic changes during sudden stratospheric warmings is presented. A brief description of the main results, obtained with the participation of the authors, using combined methods of analysis are considered. We describe procedures for the investigation of a long-term eastward displacement of the zonal ozone minimum over the Antarctic in the spring months, analysis of the spatial and temporal characteristics of the teleconnection between the tropical thermal source and the Antarctic stratosphere, and the creation of the predictive index used for the forecast of possible ozone hole anomalous development in spring months. Examples of application of analysis methods to retrieve the changes in the zonal asymmetry of the Arctic stratosphere and features of the annual ozone cycle in connection with zonal ozone asymmetry are discussed.

Keywords: data source, MERRA-2, method, ozone, reanalysis, visualization

1 Introduction

The ozone layer, located ~10–50 km above the Earth's surface, has been actively studied during the last four decades (Chubachi, 1984; Wirth, 1993; Solomon, 1999; Randel et al., 2002; Godin-Beekmann, 2010; Solomon et al., 2016; Dhomse et al., 2018; Friedel et al., 2022). The main reason for this was the development of the ozone hole in the southern polar stratosphere since the 1980s (Chubachi, 1984; Farman et al., 1985; Salby et al., 2012). Considering the important role of the ozone layer in protecting the Earth's biosphere,

its changes have been carefully studied using a global network of ground-based instruments and with the involvement of a series of satellite missions. In addition to decadal trends, stratospheric ozone undergoes significant dynamic changes due to the activity of planetary waves and the occurrence of sudden stratospheric warmings (SSWs) (Allen et al., 2003; Huck et al., 2005; Manney et al., 2015; Friedel et al., 2022; Liu et al., 2022).

Atmospheric perturbations during SSWs can be quantified from data on variations in several specific atmospheric characteristics and parameters. The de-

velopment of SSW causes changes in the horizontal and vertical distribution of temperature, pressure, geopotential height, wind direction and speed, variations of the content of small atmospheric components, including ozone, and their stratosphere-troposphere exchange (Baldwin et al., 2021). Since these processes occur under the influence of the variable activity of planetary waves (PWs), determining the characteristics of PWs is important for describing SSWs, identifying their type, assessing effects on the state of the atmosphere, and predicting possible consequences. Between atmospheric constituents, ozone is one of the most convenient components that allow investigating the PW influence on ozone distribution and dynamics, the polar vortex characteristics, the SSW events conditions, and connections of ozone changes and stratospheric temperature changes, the impact of ozone depletion and recovery on wave propagation (Hu et al., 2015).

The characteristics of PWs are obtained from the longitudinal distribution of atmospheric parameters, focusing on the main zonal wave numbers $m = 1–2$ (Baldwin et al., 2021). Data sources for the PW analysis are the archived and current series of ground and satellite measurements and the long-term series of atmospheric parameters accumulated in reanalyses (Keller & Wahl, 2021). In addition, global data from satellites and reanalyses make it possible to analyse the structure of the atmospheric layers, identify regional and local manifestations of PW, and assess the contribution to their main spectral components to atmospheric disturbances (Salby, 1982; Fleming et al., 1990; Wirth, 1993; Godin-Beekmann, 2010; Teng & Branstator, 2012; Lee & Butler, 2020). Ground-based observations are useful for studying local temporal variations and determining their possible periodicity and long-term trends due to the possibility of continuous and accurate observations at one site and at the scale of the weather station global network (Di Biagio et al., 2010; Hoffmann et al., 2011; Angot et al., 2012; Rüfenacht et al., 2012; Forkman et al., 2016; WMO, 2022).

In recent decades, multifaceted research on SSW has been ongoing, as described in key review works (Schoeberl, 1978; Hu et al., 2014; Butler et al., 2017;

Baldwin et al., 2021). Individual events have been considered as case studies (Manney et al., 2009; Chandran et al., 2011; Tao et al., 2015; Rao et al., 2018), and climatological characteristics of SSW were determined (Charlton & Polvani, 2007; de la Torre et al., 2012). Importantly, the definition of a standard criterion for SSW events has progressed (Butler & Gerber, 2018). Modelling and forecasting of SSW events also were provided (Chandran & Collins, 2014; Tripathi et al., 2016; Karpechko et al., 2018; Rao et al., 2018; Taguchi, 2018). These studies require statistical, correlative, spectral, and comparative data analysis methods and model reproduction of the observed processes.

Atmospheric dynamics during SSWs, in addition to PW effects, are also studied from the perspective of the two-way vertical troposphere–stratosphere–mesosphere coupling, covering both upward and downward propagation of perturbations and taking into account changes in the chemical composition of the air (Baldwin & Dunkerton, 2001; Huret et al., 2006; Funke et al., 2009; Kvissel et al., 2012; de Wit et al., 2014; Orsolini et al., 2017; Gardner, 2018; Ryan et al., 2018). The phenomena accompanying SSW are analysed: splitting and displacement of the stratospheric polar vortex (Solomon et al., 1985; Manney et al., 2009; Chandran & Collins, 2014; Butler et al., 2020), of the stratopause elevation (Chandran et al., 2013; France & Harvey, 2013; Limpasuvan et al., 2016; Scheffler et al., 2022), vertical movements and mesospheric intrusions (Huret et al., 2006; Manney et al., 2009; Salmi et al., 2011; Kvissel et al., 2012; Orsolini et al., 2017; Ryan et al., 2018), and impact on the weather on the Earth's surface (Baldwin & Dunkerton, 2001; Kodera et al., 2016; Yu et al., 2018; Domeisen et al., 2020; Curbelo et al., 2021; Choi et al., 2021; Hongming et al., 2022).

This work describes the main types of numerical data and techniques used in the analysis of planetary wave activity based mainly on ozone data (Sections 2 and 3). Methods of analysis of PW characteristics are described, aimed at studying PW properties and determining their role in the development of sudden stratospheric warming (Section 4). The examples of the main new results obtained through implementing the methods and approaches to analysing stratospher-

ic ozone and SSW processes are reviewed in Section 5, followed by conclusions in Section 6.

2 Measurement techniques

2.1 Instruments for ozone measurements

From the second half of the 1990s, some of the authors of this review participated in the ozone measurements in the Antarctic and Ukraine (Gritsai et al., 2000, Milinevsky et al., 2022) with the Dobson spectrophotometer and filter ozonometers, respectively. Since 2010, a Dobson spectrophotometer has been operating in Ukraine; it is involved in the worldwide network of ozone monitoring stations (Milinevsky et al., 2012). Here we briefly describe some of the instruments widely used in ozone layer research.

The current global network of ozone instruments includes ground-based sites, which were mainly established in the 1950s (due to an expansion in the use of Dobson spectrophotometers for the International Geophysical Year; Staehelin et al., 2018) and a series of satellite platforms that date back to the 1960s–1970s (SAMOS-9, 1962; Ariel-2, 1964; Nimbus-4, 1970; Nimbus-7, 1978; McPeters et al., 1998; Godin-Beekmann, 2010; see also <https://rammb.cira.colostate.edu/dev/hillger/ozone-monitoring.htm>), and (WMO, 2018; Chapter 3, page 3.69; <https://csl.noaa.gov/assessments/ozone/2018/downloads/>). In the 1990s–2010s, the series of NASA (National Aeronautics and Space Administration) satellites were replenished with EP-TOMS – Earth Probe Total Ozone Mapping Spectrometer (McPeters et al., 1998) and OMI – Ozone

Table. The satellite data used in Merged Ozone Dataset (MOD). Last Modification 21 May 2022. MOD v2 Release 1 Extended: extend OMPS NP V2.8 (equivalent to SBUV V8.7) through December 2021.
From https://acd-ext.gsfc.nasa.gov/Data_services/merged/instruments.html

Instrument	Data	Start Date	End Date	Data Usage/Comments
Nimbus 4 BUV*	5° MZM (Text) 5° MZM (HDF)	May, 1970	April, 1976	All N4 BUV data are included for historical reference, but these data should not be used for trend analysis.
Nimbus 7 SBUV	5° MZM (Text)** 5° MZM (HDF)***	November, 1978	May, 1990	All N7 SBUV data are used.
NOAA 9 SBUV/2	5° MZM (Text) 5° MZM (HDF)	February, 1985	January, 1998	No N9 SBUV/2 profile data are used. N9 SBUV/2 total column data are used only to fill gaps in 1994–1995.
NOAA 11 SBUV/2	5° MZM (Text) 5° MZM (HDF)	January, 1989	March, 2001	Apr 1995 – Sep 1997 N11 SBUV/2 data are not used.
NOAA 14 SBUV/2	5° MZM (Text) 5° MZM (HDF)	March, 1995	September, 2006	N14 SBUV/2 data after May 2000 are not used.
NOAA 16 SBUV/2	5° MZM (Text) 5° MZM (HDF)	October, 2000	May, 2014	N16 SBUV/2 data after July 2007 are not used.
NOAA 17 SBUV/2	5° MZM (Text) 5° MZM (HDF)	August, 2002	March, 2013	No N17 SBUV/2 data are used after September 2011.
NOAA 18 SBUV/2	5° MZM (Text) 5° MZM (HDF)	July, 2005	November, 2012	All N18 SBUV/2 data are used.
NOAA 19 SBUV/2	5° MZM (Text) 5° MZM (HDF)	March, 2009	Operational	No N19 SBUV/2 data are used after March 2018.
Suomi NPP OMPS	5° MZM (Text) 5° MZM (HDF)	December, 2011	Operational	All OMPS NP data after April 2012 are used.

Note: * The Nimbus-4 satellite included a sensor called the Backscatter Ultraviolet (BUV) experiment; ** Text data link: https://acd-ext.gsfc.nasa.gov/anonftp/toms/sbuv/zonal_means/MZM_N07_lyr.txt; *** HDF data link: https://acd-ext.gsfc.nasa.gov/anonftp/toms/MergedOzoneData/Ind_HDF/SBUV-Nimbus07_L3zm_v8.7-2021m0505t081704.h5.

Monitoring Instrument (Levelt et al., 2006; McPeters et al., 2008). The National Oceanic and Atmospheric Administration Solar Backscatter Ultraviolet Instrument (NOAA SBUV) series (Frith et al., 2014) was continued by OMPS – Ozone Mapping and Profiler Suite (Flynn et al., 2014); see Table (MZN – Monthly Zonal Means). GOME – Global Ozone Monitoring Experiment (Burrows et al., 1999), SCanning Imaging Absorption spectrometer for Atmospheric CHartographY – SCIAMACHY (Piters et al., 2006), and MLS – Microwave Limb Sounder (Waters et al., 2006) are also important contributors to observations for ozone studies.

Some of the listed devices are briefly described in Subsections 2.3–2.5. They are used to study changes in total ozone column (TOC) – daily, seasonal, and interannual variations, long-term trends, and global distribution, as well as to obtain and analyse vertical ozone profiles and estimates of stratosphere–troposphere exchange, in particular, during SSW events. Global satellite observations are one of the main sources to detect PW in the distribution of air constituents and study their impact on the ozone layer (Wirth, 1993; Randel et al., 2002; Huck et al., 2005).

Examples of data links for Nimbus 7 SBUV are shown in Table under ** and ***. In addition, an important direction in ozonometry is the calibration and inter-calibration of devices, comparison and verification of measurements made by different instruments, and ensuring the reliability of data and conclusions from their analysis (Bramstedt et al., 2003; McPeters et al., 2008; Antón et al., 2010).

2.2 Ground-based instruments:

Dobson spectrophotometer

Besides the Dobson spectrophotometer, other important instruments (e.g., Brewer spectrometer, ozonesonde) are successfully used for ground-based and direct ozone measurements. However, we are primarily interested here in the systems we have used. Measurement of the TOC using the Dobson spectrophotometer is based on comparing the intensity of scattered solar radiation at two wavelengths (Evans, 2008). These wavelengths are chosen to have significantly different ozone absorption coefficients. The wavelength

interval 305–340 nm is used. The difference between the selected wavelengths should not be too large; otherwise, the change in the absorption coefficient of UV radiation by the aerosol will distort the obtained value of the ozone content. Several pairs of wavelengths are used to increase the accuracy of the results.

Observations using a Dobson spectrophotometer are performed in two ways: aiming at the Sun (DS – Direct Sun) or the zenith with a cloudless (ZB – Zenith Blue) or cloudy (ZC – Zenith Cloud) sky. In the first case, when the sky is clear, the intensity of radiation from the Sun or the Moon is directly determined (the Moon in the near ultraviolet, as well as in the visible range, shines with reflected sunlight, which allows such observations to be made). In the second method, the intensity of scattered light in the direction of the zenith is registered. The basic measurements are based on the Sun; for other types (ZB, ZC), additional data reduction is performed (Evans, 2008). In particular, corrections determined by the state of cloudiness are introduced into the algorithm. A separate type of observations is based on a focused image of the Sun or Moon (FFS, FFM – filtered focused Sun and Moon, respectively).

As noted in Subsection 2.1, Ukraine operates two Dobson spectrophotometers. These Dobson spectrophotometers were used by authors for measurements of TOC in Antarctica at the Akademik Vernadsky station (hereinafter Vernadsky station) and in Ukraine at the Kyiv-Goloseyev station (Evtushevsky et al., 2008a; Milinevsky et al., 2012, Milinevsky et al., 2022). At the Vernadsky station two Dobson spectrophotometers were used – Dobson No. 031 and No. 123, at the Kyiv-Goloseyev station – Dobson No. 040. These spectrophotometers are high-precision instruments included in the international networks of global monitoring of environmental protection and control of satellite measurements: NDACC (Network for the Detection of Atmospheric Composition Change) and GAW (Global Atmosphere Watch) Program (Milinevsky et al., 2012). In the World Ozone and Ultraviolet Radiation Data Centre (WOUDC) international database, the station with device No. 040 has the name and code “Kyiv-Goloseyev STN498”. It has been operating since May 2010 as the GAW re-

gional station with the index “KGV” (<http://www.woudc.org/data/stations/>).

Observations on these two instruments provided the basis for expanding the scope of stratospheric research in Ukraine, including international cooperation with Australian and Chinese researchers. The new data on the measurement errors under different observation conditions (Gritsai et al., 2000; Evtushevsky et al., 2008a; Kravchenko et al., 2009; Grytsai & Milinevsky, 2013), the dynamics of the ozone layer (Evtushhevsky et al., 2008b; Kravchenko et al., 2012; Grytsai et al., 2017; Milinevsky et al., 2020; Milinevsky et al., 2022; Zhang et al., 2022a), and the role of planetary waves (Grytsai et al., 2005a; 2005b; Grytsai et al., 2008; Evtushevsky et al., 2015; Shi et al., 2021; Milinevsky et al., 2022; Zhang et al., 2022b) were obtained.

2.3 Satellite spectrometer TOMS

Systematic satellite measurements of ozone using Total Ozone Mapping Spectrometer (TOMS) were carried out from November 1978 to the end of December 2005. They provided data on its global distribution, spatial-temporal variations, and long-term changes (McPeters et al., 1998; Antón et al., 2010). The algorithm for converting the results of measurements of the intensity of scattered solar ultraviolet (UV) radiation into values of the total ozone column has been modified from time to time (Antón et al., 2010). The basic algorithm TOMS version 8 (V8) uses two wavelengths to calculate the TOC: a wavelength with weak absorption (331.2 nm) to estimate the effective surface reflectance (or effective cloud fraction) and another wavelength (317.5 nm) with stronger absorption. An implicit assumption is made of no significant variation in effective reflectivity or cloud fraction between 331.2 and 317.5 nm. An inverse remote sensing algorithm is used. The ozone profile is considered, which is selected for a given latitude and month from 3–10 profiles, depending on the values of TOC.

Measurement data obtained by three satellites with the TOMS spectrometer on board are freely available: Nimbus-7 (1978–1993), Meteor-3 (1991–1994), and Earth Probe (1996–2005). The website <https://ozoneaq.gsfc.nasa.gov/data/ozone/> provides daily data

of global measurements by the TOMS spectrometers from 1 November 1978 to 31 December 2005 inclusive. It should be noted that according to the given chronology of the TOMS operation, a data gap covers 1993–1995 as Meteor-3 data was not presented in the V8 algorithm.

2.4 Satellite spectrometer OMI

Since 2006, Ozone Monitoring Instrument has been used to monitor ozone. OMI is a spectrometer for nadir observations in the UV and visible range (McPeters et al., 2008). It is installed on-board the Aura satellite as part of the NASA Earth Observing System (EOS; <http://eospso.gsfc.nasa.gov/>). OMI continues to record ozone and other atmospheric parameters (<https://ozoneaq.gsfc.nasa.gov/data/ozone/#>) related to ozone chemistry and climate performed by the earlier TOMS spectrometers.

OMI measurements cover three spectral ranges: visible, 350–500 nm; UV1, 270–312 nm; UV2, 306–380 nm, with a spectral resolution between 0.42 nm and 0.63 nm. The field of view in the nadir is 13×24 km for TOC measurements and 13×48 km for vertical ozone profiles. OMI data are available on the Tropospheric Emission Monitoring Internet Service (TEMIS) website <https://www.temis.nl/protocols/O3total.php>. In addition to the ozone measurement, the concentration of other constituents, including CO, NO₂, SO₂, Br₂O, HCHO, and aerosols is also determined (<https://aura.gsfc.nasa.gov/science/gallery-omi.html>).

2.5 Satellite microwave radiometer MLS

Satellite measurements by the Microwave Limb Sounder (MLS) are carried out on board the Aura spacecraft, which is a part of the NASA EOS satellite system (Waters et al., 2006). MLS measurements began in August 2004 and are still ongoing. The main mission of the MLS instrument is to measure atmospheric ozone and air quality and assess the state of the climate. MLS measures atmospheric temperature profiles spanning the troposphere to thermosphere and profiles of more than a dozen atmospheric components, including O₃ and CO, as well as cloud water and ice content.

The MLS radiometer has a spatial resolution of 200–300 km along-track, 7 km across-track, and 3–4 km vertically (Livesey et al., 2022). It makes two observations daily (day and night) along the noon–midnight meridian. MLS data on atmospheric temperature, geopotential heights, and volume mixing ratio (VMR) of CO and ozone are among the main sources of information used for the study of SSWs (Shi et al., 2020; 2021; Wang et al., 2019; 2021). Zonal wind data are not presented in the MLS measurements but may be calculated from the geopotential height and temperature fields using the geostrophic approximation (Fleming et al., 1990). The recommended useful vertical range for ozone measurements is from 215 to 0.00564 hPa (Livesey et al., 2022).

CO values from MLS measurements were compared with data from the microwave radiometer (MWR) in Kharkiv (Wang et al., 2019). Compared to the Kharkiv MWR, which estimates CO using the 115.3 GHz emission line, the MLS CO data are obtained from measurements of two bands, 240 and 640 GHz (Livesey et al., 2022). Estimated accuracy is about $\pm 30\%$ at levels from 215 to 100 hPa, $\pm 10\%$ at 10 hPa, and up to 50% at levels from 1 to 0.0022 hPa; at levels above 0.0022 hPa and below 215 hPa, the CO data are not recommended for use (Livesey et al., 2022).

3 Reanalyses and Model Outputs

Reanalyses are secondary synthesized data obtained by assimilating the results of historical observations with the guidance of physical models. They provide an important tool for studying the climate and its changes in recent decades based on air temperature, geopotential height, ozone, CO, precipitable water vapor, specific humidity, aerosols, and other atmospheric variables (Keller & Wahl, 2021; also see Subsections 3.1–3.5 below). The use of these data focuses on the quality and coverage of the observational data used to generate the reanalyses. The adequacy of the spatial and temporal resolution of the output fields studying the physical processes is under consideration. The comprehensive description of existing reanalyses is presented in NCAR, climate data guide (<https://climatedataguide.ucar.edu/climate-data/atmospheric-reanalysis-overview-comparison-tables>).

Reanalyses assimilate a number of atmospheric variables into a forecast model, which allows evaluating the climate state, overview and comparison.

3.1 Reanalysis NCEP–NCAR

The NCEP–NCAR reanalysis of the National Centers for Environmental Prediction (NCEP) / National Center for Atmospheric Research (NCAR) was developed in 1991 in cooperation, in particular, with the European Center for Medium-Range Weather Forecasts (ECMWF) based on the climate data assimilation system (Climate Data Assimilation System, CDAS), which covers the period from 1948 to the present (Kalnay et al., 1996). The development of the reanalysis was supported by the global program of the National Oceanic and Atmospheric Administration (NOAA). Data from the reanalysis are available on the NOAA website <https://psl.noaa.gov/data/gridded/data.ncep.reanalysis.html>.

The data assimilation model in the reanalysis has an equivalent horizontal resolution of about 210 km or $2.5^\circ \times 2.5^\circ$ in the latitude–longitude grid and 17 vertical pressure levels from 1000 to 10 hPa. The most reliable data in the reanalysis are presented for the satellite era since 1979, when global coverage of satellite measurements was introduced. During 1948–1957, little atmospheric observational data were available, and most of this was from the Northern Hemisphere, so the reanalysis data for this period are less usable (Kistler et al., 2001).

The NCEP–NCAR reanalysis provides users with many convenient tools for analysing the data series used, which other reanalyses do not provide. In our work, the analytical capabilities of the NCEP–NCAR reanalysis contributed to the rapid visualization of data and the optimal choice of the type of graphical representation. This accelerated obtaining the necessary results and, in this way, significantly increased research productivity. Particular examples are now discussed.

1) *Monthly/Seasonal Climate Composite*. Plots of monthly and seasonal composites of variables (mean, anomalous,

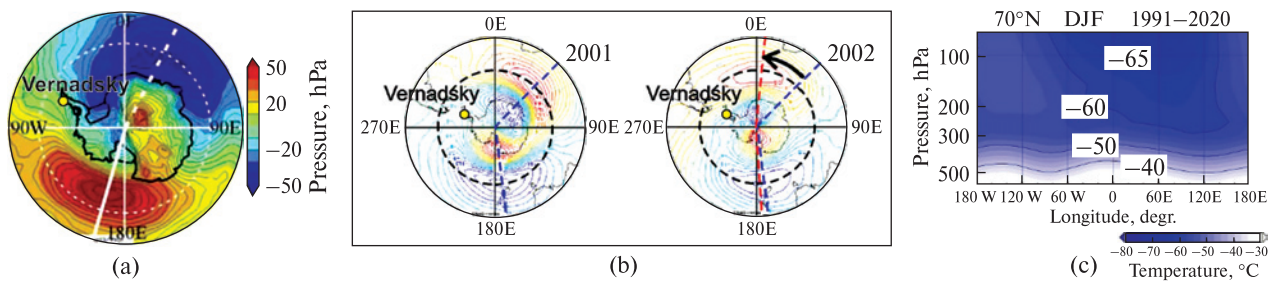


Figure 1. (a) Monthly mean distribution of tropopause pressure anomalies in the Southern Hemisphere in October 2006 (Evtushevsky et al., 2008b), (b) longitudinal displacement of zonal wind anomalies (dashed radial lines) at a pressure level of 30 hPa, averaged over September–November for conditions of a strong (2001, left) and weak (2002, right) stratospheric polar vortex over Antarctica, modified after (Grytsai et al., 2008), (c) longitude–pressure section of air temperature at 70°N latitude: climatology for December–February averaged over 1991–2020, data from NCEP/NCAR reanalysis (<https://psl.noaa.gov/data/reanalysis/reanalysis.shtml>)

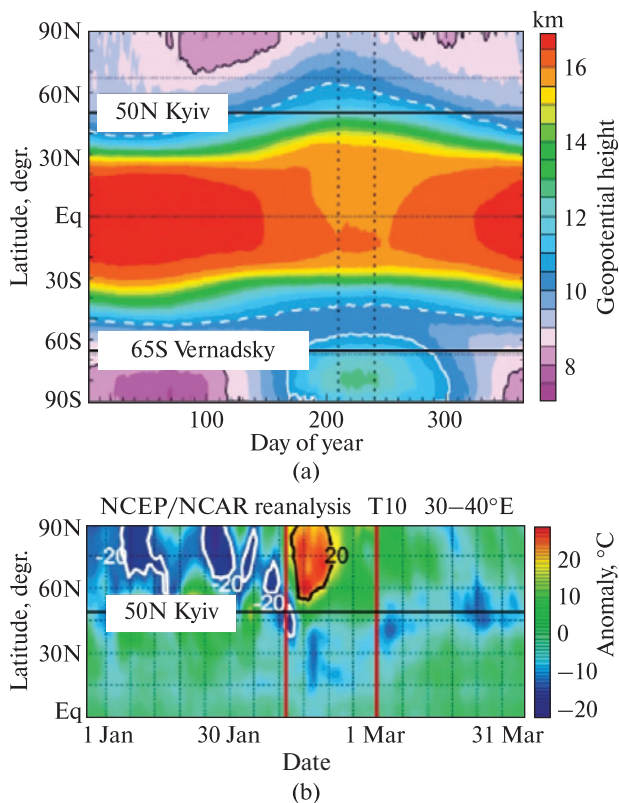


Figure 2. (a) Seasonal variation of zonal mean tropopause geopotential height (in km) between 90°N and 90°S over the year: 30-year climatology averaged over 1979–2008 (by data from <https://psl.noaa.gov/data/reanalysis/reanalysis.shtml>) and (b) time-latitude diagram of temperature anomalies (relative to climatology 1981–2010) at a pressure level of 10 hPa in the sector 30°–40°E during the sudden stratospheric warming in February 2018, modified after (Wang et al., 2021)

lies, and long-term means). Lat/Lon plots for any desired region and height cross sections are available (<https://psl.noaa.gov/cgi-bin/data/composites/printpage.pl>).

Figure 1 shows options for averaging the investigated parameters by selected indicators with their graphic reproduction on the reanalysis site: (a, b) tropopause parameters in the Southern Hemisphere in the polar projection (Evtushevsky et al., 2008b; Grytsai et al., 2008) and (c) vertical distribution of air temperature along the latitude circle 70°N.

2) *Time Section Plots Using Gridded Daily Data, Hovmöller.* Time-latitude (Fig. 2) and longitude–time sections are available at https://psl.noaa.gov/map/time_plot/.

3) *Extract time series: Monthly/Seasonal (ASCII).* Tables ‘year – month’ in rows and columns, respectively, are available at <https://psl.noaa.gov/cgi-bin/data/timeseries/timeseries1.pl>. Figure 3 shows a screenshot of a fragment of one of the tables.

4) *Linear Correlations in Atmospheric Seasonal/Monthly Averages.* This allows the creation of a plot of monthly and seasonal correlations of a gridded variable with ocean/atmosphere index time series. The user can also input a time series for analysis (<https://psl.noaa.gov/data/correlation/>). This type of analysis allows the user to plot the distribution of the correlation of the field of an atmospheric variable with climate indices or with a given custom index (adjacent to time). The custom index created by the user is placed on the anonymous ftp server <ftp.cdc.noaa.gov>

2007	27.707	17.322	14.121	7.331	1.064	-4.109	-3.486	1.358	7.752	9.114	12.340	20.775
2008	26.256	19.839	8.608	3.405	-0.513	-2.385	-2.517	0.805	5.469	12.521	15.343	20.165
2009	22.275	-0.895	8.122	10.420	1.712	-3.419	-3.686	1.540	6.604	10.926	10.618	15.064
2010	17.960	2.421	8.818	4.112	-0.892	-0.925	-1.427	1.647	6.131	9.861	15.770	17.958
2011	18.614	25.981	23.419	2.826	-3.470	-3.910	-2.330	1.101	6.354	10.737	20.695	27.489
2012	19.772	9.117	11.793	3.467	0.278	-4.019	-1.916	2.552	6.927	10.629	18.576	13.412
2013	6.662	5.341	13.813	14.820	2.117	-2.888	-2.899	1.638	5.842	10.592	18.726	25.884
2014	24.921	19.787	16.984	5.378	-1.635	-3.156	-2.423	1.016	6.421	10.879	13.510	21.772
2015	19.865	22.246	21.718	2.424	-2.364	-3.283	-2.758	1.657	6.596	11.552	20.842	29.668
2016	25.150	23.158	4.685	-1.292	-0.483	-2.051	-1.678	1.645	4.455	7.845	9.916	19.062
2017	21.303	14.412	9.103	4.868	0.171	-1.330	-0.728	1.616	5.600	10.880	16.352	14.824
2018	23.849	11.971	10.920	4.292	0.785	-3.064	-1.052	2.476	6.239	10.708	15.226	15.021
2019	6.857	10.123	18.769	10.445	-3.441	-3.418	-2.562	0.454	5.778	11.021	16.837	19.161
2020	30.181	32.467	31.786	16.172	-0.418	-3.925	-3.119	1.362	7.120	10.057	19.451	20.630
2021	6.342	13.444	18.411	13.243	3.290	-2.006	-0.996	0.738	-999.999	-999.999	-999.999	-999.999
-999.999												
50mb Pressure Level u wind (m/s)												
Latitude Range used: 60.0 to 60.0												
Longitude Range used: 0.0 to 357.5												
NCEP Reanalysis												
Produced at NOAA PSL at https://psl.noaa.gov/data/timeseries/												
Climatology, if used, is 1981-2010.												
Date submitted: 9/28/2021 at 01:30												

Figure 3. Interannual changes in the mean zonal wind speed at 60°N latitude, 50 hPa according to NCEP–NCAR reanalysis data. Fragment of a screenshot of the monthly time series from <https://psl.noaa.gov/cgi-bin/data/timeseries1.pl>

Home » Plotting & Analysis » Monthly/Seasonal Correlations » Custom Time-series

Custom time series directions

Note: I recently found out that the FTP files could potentially be deleted after 2 days. If this is a problem please email me. I am looking into ways of changing this.

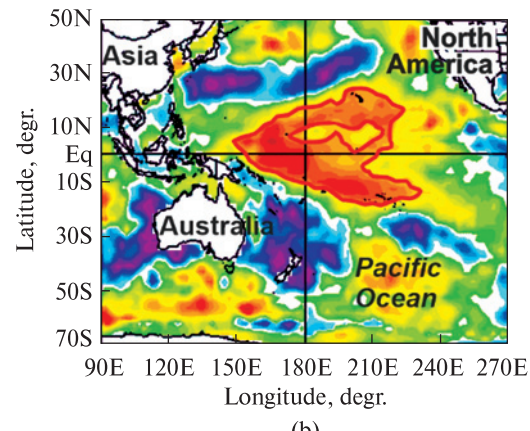
To use your own time series, you place the file in PSL's anonymos ftp server. Type ftp [ftp.cdc.noaa.gov](ftp://ftp.cdc.noaa.gov) and use anonymous as the login name and your email as the password. Or, use an ftp application of your choice. Then, cd to /Public/incoming/timeseries/ and put the file there. You won't be able to edit or delete the file.

For name of file from the webpage, use /Public/incoming/timeseries/filename. Make sure the full path is specified and is spelled EXACTLY as shown or you will get an error.

```
year1   yearend
year1   janval febval marval aprval mayval junval julval augval sepval octval novval decval
year2   etc.
yearend janval febval marval aprval mayval junval julval augval sepval octval novval decval
missingvalue
```

Note that years should be 4 digit integers. There should be at least one space between values. If a

(a)



(b)

Figure 4. (a) Screenshot of the NCEP–NCAR reanalysis page explaining how and in what format to download a chosen time series from <https://psl.noaa.gov/data/correlation/custom.html>. (b) Example to illustrate the longitude–latitude distribution of the correlation between the sea surface temperature in the tropics in June and the stratospheric temperature index in October created for the Western Hemisphere segment over Antarctica. A graphical presentation of the correlation is obtained from the webpage <https://psl.noaa.gov/data/correlation>

to /Public/incoming/timeseries/ and when computing the correlation, downloaded from <https://psl.noaa.gov/data/correlation/custom.html> by selecting ‘If custom:’ (Fig. 4a) on the reanalysis website. Figure 4b shows an example of the use of this analysis

tool. An example of correlation calculations is presented at <https://www.psl.noaa.gov/data/writ/ocean.example.usetime.html>.

5) *Other atmospheric parameters.* The NCEP–NCAR reanalysis also provides for the use of climate indices

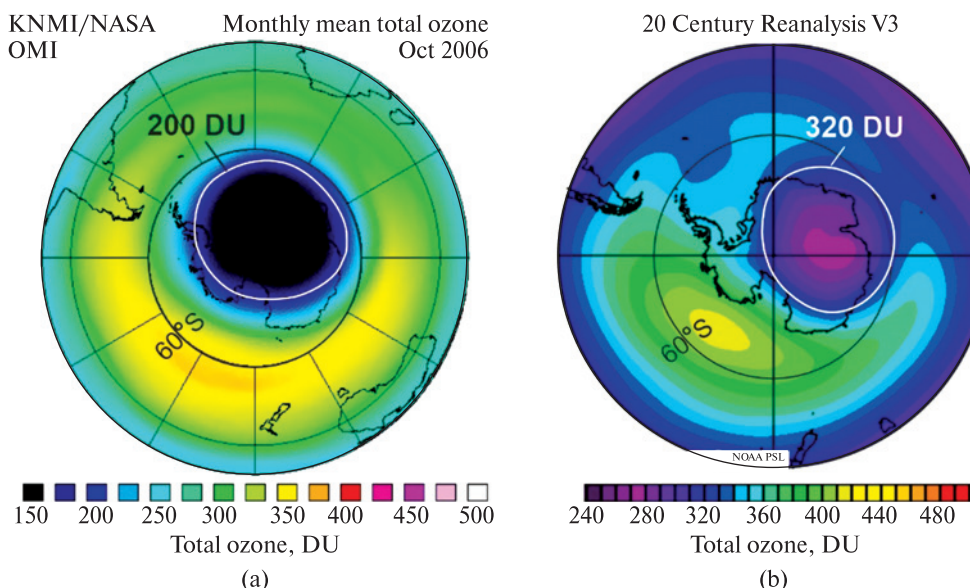


Figure 5. Distribution of total ozone column in the Southern Hemisphere in October 2006 with an ozone hole over Antarctica according to (a) OMI satellite spectrometer data (https://www.temis.nl/protocols/o3field/o3mean_omi.php) and (b) 20th Century Reanalysis Version 3 (20CRv3, <https://psl.noaa.gov/cgi-bin/data/composites/plot20thc.v2.pl>). The overestimation of the TOC in the region of the ozone hole in the reanalysis compared to the OMI is ~120 DU (white contours). The KNMI – Royal Netherlands Meteorological Institute

of atmospheric variability (<https://psl.noaa.gov/data/climateindices/>), including the Niño regions, the Arctic and Antarctic Oscillations (AO and AAO, respectively), the Quasi-Biennial Oscillation (QBO), the Southern Oscillation Index (SOI), the North Atlantic Oscillation (NAO), and the Pacific Decadal Oscillation in the Pacific Ocean (PDO).

El Niño–La Niña phenomena are represented by anomalies of atmospheric variables comparing both phenomena by samples of years with their maximum phase, separately for winter and spring seasons (<https://psl.noaa.gov/enso/compare/>). It is also possible to analyse the latitude–daily height distribution of the Eliassen–Palm flux vector (<https://psl.noaa.gov/data/epflux/>).

A significant limitation in using the NCEP–NCAR reanalysis for middle atmosphere studies is its minimum pressure level of 10 hPa (~32 km, corresponding to the middle stratosphere). In comparison, for the Modern-Era Retrospective Analysis for Research and Applications (MERRA-2) reanalysis (discussed in Section 3.2 below), the upper-pressure surface of the

standard output is at 0.1 hPa (~64 km, in the lower mesosphere). Actually, model data from MERRA-2 are available up to ~87 km, but only for temperature and geopotential height.

The MLS satellite provides reliable data up to ~90 km (see Section 2.5) – this is the mesopause region. Because of the necessary limitations in the spatial and temporal extents of the available data, investigation of SSW processes that cover the full atmospheric extent from the troposphere to the mesosphere has only been possible in the past few decades.

To expand the time limits of research, the 20th Century Reanalysis (20CR) was developed, which covers the entire 20th and most of the 19th centuries (http://apdrc.soest.hawaii.edu/datadoc/20century_reanalysisV3.php, see also https://psl.noaa.gov/data/20thC_Rean/). This is a product of NOAA and the University of Colorado, USA (Slivinski et al., 2021). It has monthly mean geographic distributions of total ozone (up to 2015, <https://psl.noaa.gov/cgi-bin/data/composites/plot20thc.v2.pl>). However, in some cases, these data show significant differences between 20CR

and satellite measurements. It can be seen from Figure 5 that although the nature of asymmetry in the distribution of TOC is generally consistent, the range of TOC according to OMI data is 150–370 Dobson units (DU) (Fig. 5a), but is considerably overestimated in 20CR version 3 at 270–420 DU (see Fig. 5b). We also should mention an ECMWF (ERA-20C) version of the 20CR (<https://www.ecmwf.int/en/forecasts/dataset/ecmwf-reanalysis-20th-century-ii>).

3.2 Reanalysis MERRA-2

Version 2 of the MERRA-2 is the latest version of the 4th generation atmospheric reanalysis developed by NASA (Gelaro et al., 2017). It uses long-term meteorological data series to inform an improved atmospheric circulation model. The output covers the period from 1980 to the present and has a spatial resolution of 0.5° in latitude and 0.625° in longitude with 42 vertical pressure levels from the surface to 0.1 hPa (<https://gmao.gsfc.nasa.gov/reanalysis/MERRA-2/>). In spatial resolution and vertical extent, MERRA-2 has advantages over the NCEP–NCAR reanalysis ($2.5^\circ \times 2.5^\circ$ in the latitude–longitude grid and 17 vertical pressure levels from 1000 to 10 hPa, see Subsection 3.1). Visualizations of average monthly data, climatology, and anomalies are available (https://fluid.nccs.nasa.gov/reanalysis/anomaly_merra2/). However, many of the analysis tools available in the NCEP–NCAR reanalysis (Subsection 3.1) are not present in MERRA-2.

3.3 ECMWF Reanalysis

The ECMWF reanalysis produced several important global reanalyses. A key data set has been ERA-Interim which provided a global reanalysis covering the satellite period from 1979 to 2019 (Dee et al., 2011; <https://www.ecmwf.int/en/forecasts/dataset/ecmwf-reanalysis-interim>). Since 2019, this has been superseded by the ERA5 reanalysis (Hersbach et al., 2020; <https://www.ecmwf.int/en/forecasts/datasets/reanalysis-datasets/era5>). Both ERA-Interim and ERA5 are derived from the ECMWF Integrated Forecast System (IFS). The IFS uses 4D variation analysis with

a 12-hour analysis window. The reanalyses provide 3D data of the main atmospheric parameters (temperature, geopotential height, wind, water vapour, and ozone) and other important parameters on clouds, radiation, and surface properties. The ERA5 reanalysis covers the period from January 1950 to the present, with data presented on a ~ 30 km grid for 37 levels from the surface to 1 hPa (~ 48 km).

3.4 Ozone in multi-sensor reanalysis MSR

Multi-Sensor Reanalysis of ozone data (Multi-Sensor Reanalysis – MSR) is TOC data set constructed using the assimilation of all available series of ozone satellite observations, including data from TOMS (on board the Nimbus-7 and Earth Probe satellites), SBUV (Nimbus-7, NOAA-9, NOAA-11, and NOAA-16), SCIAMACHY (Envisat), OMI (EOS-Aura), GOME (ERS-2) and GOME-2 (Metop-A) and ground measurements by Dobson spectrophotometer and Brewer spectrometer with further model data processing (van der A et al., 2010). Combined satellite observations were assimilated using a chemical transport model based on ECMWF meteorological data (van der A et al., 2010). The daily and monthly means of the global O_3 fields and overpass data in MSR-2 are presented at https://www.temis.nl/protocols/o3field/o3month_msr2.php and cover the period 1970–2021. The data on trace gases and air pollution are also presented. Near-real-time global ozone fields, archives of individual instruments, and overpass data are provided in the TEMIS project (see Section 2.3 above) at <https://www.temis.nl/protocols/O3global.php>.

3.5 Ozone in SBUV MOD reanalysis

The merged series of ozone data Merged Ozone Data (MOD) is based on satellite measurements by ultraviolet radiometers SBUV and SBUV/2 (SBUV MOD; Frith et al., 2014; see also Table). The SBUV MOD reanalysis presents vertical profiles of ozone in the form of (1) zonal-averaged data for 5-degree latitude intervals and (2) daily local data for individual ground stations derived from overpass measurements of the satellite instrument (<https://acd-ext.gsfc.nasa.gov/>)

[Data_services/merged/index.html](https://acd-ext.gsfc.nasa.gov/Data_services/merged/index.html)). The data are available in Version 8.7 for January 1970 to December 2021 (https://acd-ext.gsfc.nasa.gov/Data_services/merged/previous_mods.html).

The last MOD modification dated 21 May 2022, v2 Release 1 Extended, is currently implemented. The overpass data contains information for nine atmospheric layers. Seven layers with a step of about 3 km in height are located between 25 hPa and 1 hPa (26–48 km) and characterize the middle and upper stratosphere (up to the stratopause). The combined layers 1–8 (below 25 km) and 16–21 (above 48 km – to the upper limit of the atmosphere) cover the troposphere–lower stratosphere and mesosphere, respectively (<https://acd-ext.gsfc.nasa.gov/anonftp/toms/sbuv/MERGED/>). The zonal mean data are similarly arranged and available at https://acd-ext.gsfc.nasa.gov/Data_services/merged/data/sbuv_v87_mod.int_lyr.70-20.za.r1.txt.

Another type of ozone overpasses contains daily profiles at specified stations formed from all instruments (Nimbus BUV – NOAA SBUV – OMPS) aggregated into a single file (<https://acd-ext.gsfc.nasa.gov/anonftp/toms/sbuv/AGGREGATED/>). These profiles include ozone data for each layer from 1 to 21 (1013–0.1 hPa, or 0–64 km) with a steady height step, so they have the advantage of a more detailed reproduction of the vertical ozone distribution. Each type of data, besides the profile, also provides a value of TOC.

3.6 Ozone in climate models

The Chemistry Climate Model Initiative (CCMI) is an international project that coordinates developing and evaluating advanced climate models (Eyring et al., 2016).

CCMI models simulate physical and chemical processes in the lower and middle atmosphere and provide a more robust simulation of atmospheric change than models using prescribed atmospheric chemistry (<https://www.wcrp-climate.org/wgcm-cmip/wgcm-cmip6>). A series of simulations were conducted by a range of climate models (including coupled ocean-atmosphere models) under phase 2 of CCMI (CCMI-2) for the 6th Coupled Model Intercomparison Project (CMIP6). These simulations, which represent the current state-of-the-art climate modelling, provided free-

running and dynamically-constrained output covering the historical period from 1980 to 2014. The output includes vertical profiles of ozone volume mixing ratio from the surface to the mesopause region, with a typical spatial resolution of ~2° in latitude and longitude.

Thanks to considerable progress in the simulation of processes with associated stratospheric ozone in recent decades (Dhomse et al., 2018), the short-term spatial representation of polar ozone fields and their interaction with planetary waves is an area where further model improvement is needed. In a study by Ivaniha (2020), a comparison of the amplitude of the zonal asymmetry in the TOC over the Antarctic showed that a selection of CMIP6 models tended to underestimate the asymmetry by 42% compared to the MERRA-2 reanalysis. This study highlights that significant biases can be present in the vertical and horizontal distribution of simulated ozone in the polar regions, which has potential implications for flow-on effects on temperature and chemical processes in the lower polar stratosphere.

4 Analysis methods

The behavior of planetary waves in the atmosphere is described using versatile approaches that allow to select the analysis method and the basic atmospheric parameters. An integral characteristic of the PW is the Eliassen–Palm (EP) vector flux. The EP flux theory is based on thermodynamic equations (Tanaka et al., 2004).

The vertical EP flux is an important diagnostic indicator of the nature of PW propagation and the “wave–mean flow” interaction (Dwyer & O’Gorman, 2017). The averaged data show that the maximum EP flux up through the troposphere occurs in the middle latitudes of both hemispheres (43–50°N and 50–55°S (Dwyer & O’Gorman, 2017)). The meridional location of the maximum tropospheric westerly winds affects where the wave flux is deflected as it rises into the stratosphere, poleward or equatorward (Dwyer & O’Gorman, 2017). Vector diagrams of the EP flux in the meridional plane make it possible to trace changes in wave activity and the direction of its propagation (Fig. 6a and 6b).

Diagrams in Figure 6a provide a general idea of the vertical transport of wave energy between the troposphere and the stratosphere and data on its interannual changes. They are useful in analysing and comparing the development of PW activity in the meridional plane in individual SSW events (Fig. 6b). Momentum flux and heat flux, which are components of the EP flux, are also used to describe the averaged characteristics of atmospheric dynamics (Dwyer & O’Gorman, 2017).

4.1 Spectral Fourier analysis

More detailed data on planetary waves are obtained by analysing their spectral composition and the amplitude of the spectral components. Important manifestations of PW are meridional deviations of atmospheric masses relative to a certain latitude circle and zonal asymmetry in the horizontal distribution of atmospheric variables (see Fig. 1). Therefore, one of the ways of studying the PW spectra is the analysis of disturbances (deviations) in the longitudinal distribution of the studied parameters (mainly temperature, zonal wind, geopotential height, and ozone).

In addition, a statistical description of the characteristics of planetary waves is carried out with the determination of average amplitudes, phases, long-term trends, and abnormal values, as well as periodicity, using Fourier and wavelet analysis.

For a detailed description of the spectra of planetary waves using satellite measurements of the TOC, we used the long-term longitudinal distribution $f(\lambda)$ decomposition on the spectral components (Fourier analysis) with zonal numbers m (Grytsai et al., 2005b; Pinsky, 2009; Constantin, 2016):

$$f(\lambda) = \sum_{m=-\infty}^{\infty} a_m e^{im\lambda},$$

$$a_m = \frac{1}{2\pi} \int_{-\pi}^{\pi} f(\lambda) e^{-im\lambda} d\lambda.$$

Averaging the daily amplitudes for the selected time interval with a duration of N days, we get the amplitude of the wave $A_{m\text{gen}}$, which characterizes the total

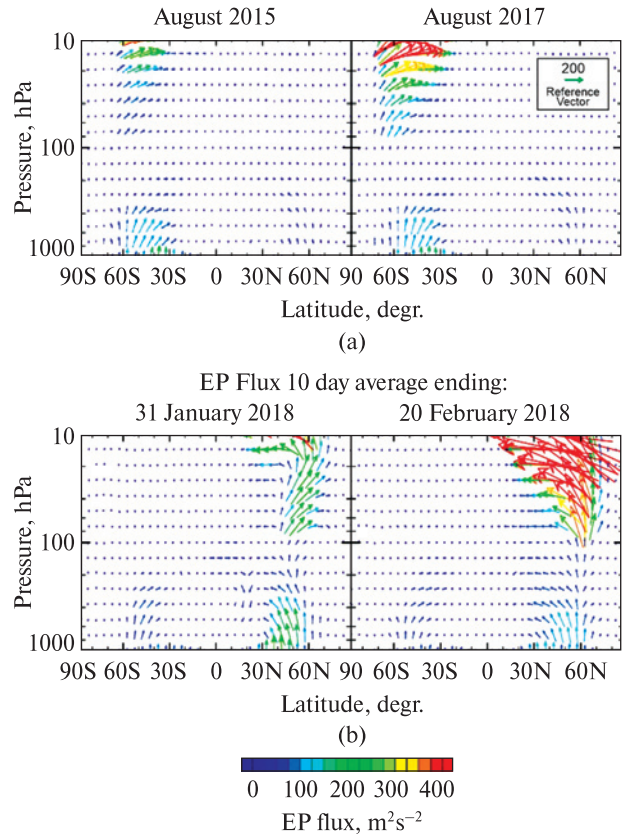


Figure 6. (a) Eliassen–Palm flux in the Southern Hemisphere in August 2015 and 2017 (Kravchenko et al., 2018) and (b) in late January (left) and mid-February (right) 2018 before and during the major SSW, respectively, in the Arctic stratosphere according to NCEP–NCAR reanalysis data (<https://psl.noaa.gov/data/epflux/>)

contribution to the disturbance of traveling and stationary component of planetary wave:

$$A_{m\text{gen}} = \frac{1}{\pi N} \sum_{j=1}^N \left| \int_{-\pi}^{\pi} f_j(\lambda) e^{-im\lambda} d\lambda \right|.$$

Averaging daily longitudinal profiles for N days (most often during a month or during a season (three months)), we determine the amplitude of the stationary component $A_{m\text{st}}$:

$$A_{m\text{st}} = \frac{1}{\pi N} \left| \sum_{j=1}^N \int_{-\pi}^{\pi} f_j(\lambda) e^{-im\lambda} d\lambda \right|.$$

4.2 Spectrum of planetary waves in Antarctic ozone

In this subsection, we describe the examples of processing techniques considered above. Figures 7 and 8 illustrate processing techniques for PW spectrum analysis. Figure 7a shows an example of the longitudinal distribution of TOC at latitude 65°S for one date, October 15, 1996 (top) and an example of selecting spectral components $m = 1–5$ (in the middle) retrieved by spectral Fourier analysis method. The observed longitudinal profile is compared with the one reconstructed by the sum of five components (Fig. 7a, bottom). The difference between these two profiles exhibits the root-mean-square deviation ~ 6.9 DU or 2.5% of the TOC mean value (Grytsai et al., 2005b).

The two images in Figure 7b demonstrate the use of the method of visualization of changes in the TOC distribution at the same latitude of 65°S in the “longitude-date” coordinates (Grytsai et al., 2005a; 2022). The edge region of the stratospheric polar vortex and the ozone hole is located near the 65°S latitude circle (Grytsai et al., 2005c). Therefore, the diagram in Figure 7b reflects both the nature of zonal movements at the edge of the vortex under the influence of planetary waves and the duration of wave activity. The slope of the bands on the diagrams shows that the waves are moving to the East, and their clear time sequence in

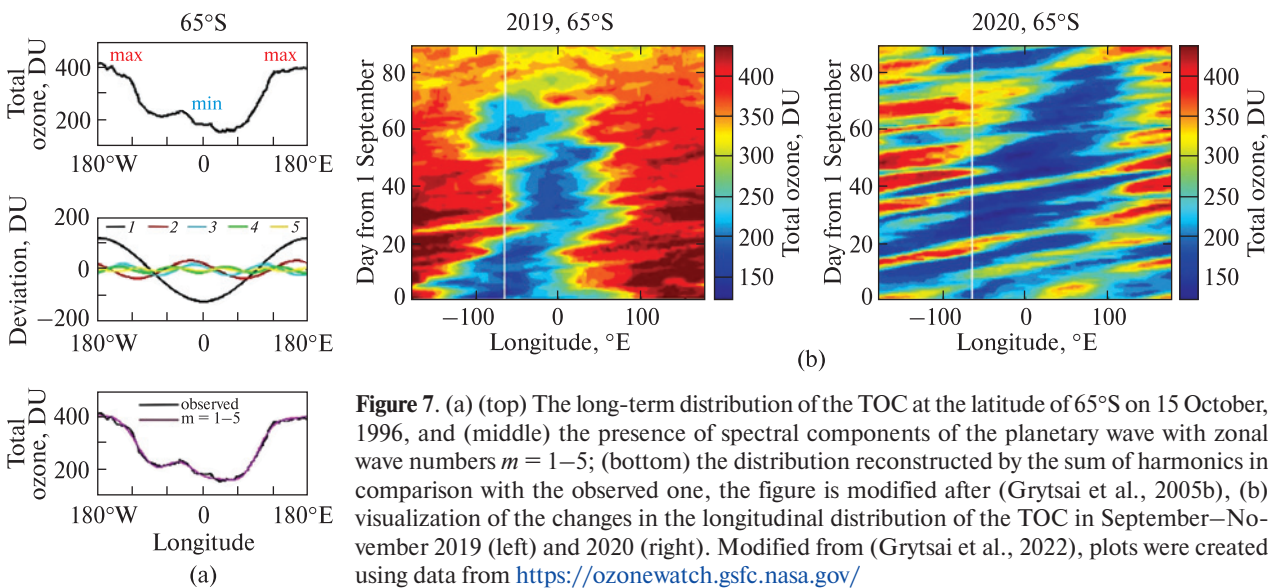


Figure 7. (a) (top) The long-term distribution of the TOC at the latitude of 65°S on 15 October, 1996, and (middle) the presence of spectral components of the planetary wave with zonal wave numbers $m = 1–5$; (bottom) the distribution reconstructed by the sum of harmonics in comparison with the observed one, the figure is modified after (Grytsai et al., 2005b), (b) visualization of the changes in the longitudinal distribution of the TOC in September–November 2019 (left) and 2020 (right). Modified from (Grytsai et al., 2022), plots were created using data from <https://ozonewatch.gsfc.nasa.gov/>

September–October 1996 (Fig. 7b, left) allows the period of oscillations to be estimated as seven days. In 1996 at latitude 65°S, the longitudinal shifts of maxima and minima of TOC lasted until November, and in 2002 only until September (Fig. 7b, left and right, respectively). The difference in the time of disappearance of zonal waves allows us to conclude a significantly shorter duration of the existence of the polar vortex in the second case, that is, about an earlier date of stratospheric warming after the collapse of the vortex.

Therefore, the combination of spectral analysis and visualization of the longitudinal distribution of the TOC (Fig. 7) gives a more detailed description of the contribution of planetary waves to the processes of development of the ozone hole and stratospheric polar vortex.

Figure 8 shows other techniques of analysis and graphical representation of the spectral characteristics of zonal waves in the ozone distribution over the Antarctic. Two families of curves in Figure 8a illustrate the interannual variability of the amplitude and phase of zonal waves $m = 1$ and $m = 2$, and the curves and approximation lines in Figure 8b show interannual variations and linear trends of their phase (Grytsai et al., 2005c).

An interesting result was obtained when analysing the ratio “wave amplitude A /zonal number m ” (Fig. 8c) (Grytsai, 2011). Both axes of Figure 8c are built on a logarithmic scale, and this presentation reveals an al-

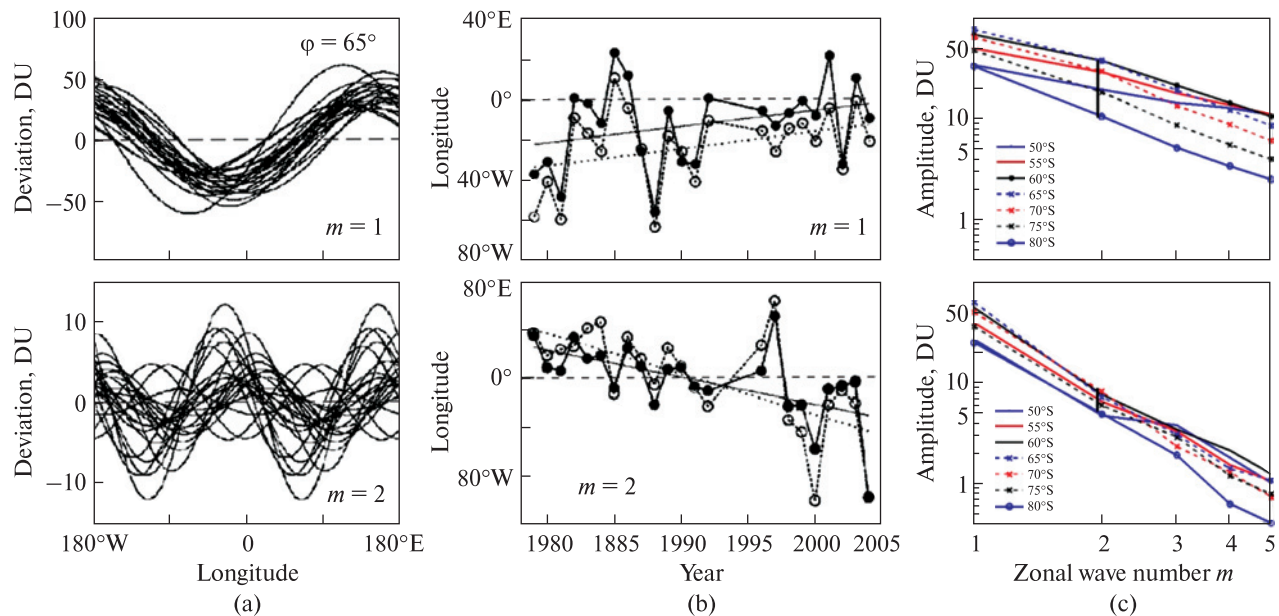


Figure 8. (a) Interannual variations of the amplitude and phase of stationary zonal waves $m = 1$ and $m = 2$ in the distribution of TOC at the latitude of 65°S in 1979–2004 and (b) the interannual variations and long-term trends of their phase. Figures are modified after (Grytsai et al., 2005c). (c) Dependence of the wave amplitude on the zonal number $m = 1\text{--}5$; latitudes $50\text{--}80^{\circ}\text{S}$, period 1979–2021; thick vertical lines indicate the change in the amplitude range of wave $m = 2$ when moving from averaging daily values (including running and stationary components, top) to monthly or seasonal average values (stationary component, bottom)

most linear power-law dependence of the amplitude A on m : $A \sim m^{-k}$. However, the exponent for the stationary wave is significantly higher with $k = 1.9\text{--}2.6$ for the total wave with $k = 0.7\text{--}1.6$. Therefore, harmonic $m = 1$ turns out to be dominant in the stationary wave, and harmonics $m = 2\text{--}5$ are significantly weaker compared to the case of the total wave (separated by vertical lines in Figure 8c at the bottom and top, respectively). In general, the representation of the linear form of the power dependence “wave amplitude A – zonal number m ” in Figure 8c turned out to be productive because it indicates the non-randomness of the relationship between harmonics, and this relationship deserves a more detailed study.

5 Main results of the use of data, their processing, and analysis

One of the most cited results is the retrieval of long-term changes in the zonal asymmetry of ozone over Antarctica in the spring (September–November) when

PW activity increases maximally (Grytsai et al., 2007). The analysis methods included the construction of the longitudinal distributions of the TOC (Fig. 7a) at separate latitude circles within $50\text{--}80^{\circ}\text{S}$ (Fig. 9), which gave an advantage in detecting a new effect. Polynomial fitting was applied, and the eastward displacement of the zonal minimum of the TOC was established by comparing its longitude from the beginning of satellite measurements (1979) to the 2000s (Fig. 9). The previously unknown process of long-term geographical redistribution of the zonally asymmetric TOC is related to the thermal state of the Antarctic stratosphere, the propagation of planetary waves, and the long-term trend of TOC itself (Salby et al., 2012; Solomon et al., 2016) due to ozone depletion and recovery of the ozone layer from the 1980s to the 2010s (Grytsai et al., 2017). An eastward shift described in (Grytsai et al., 2007) was confirmed by Agosta and Canziani (2010) and Siddaway et al. (2020) for the ozone minimum location, and by Lin et al. (2009) for the phase of wave 1 in stratospheric temperature.

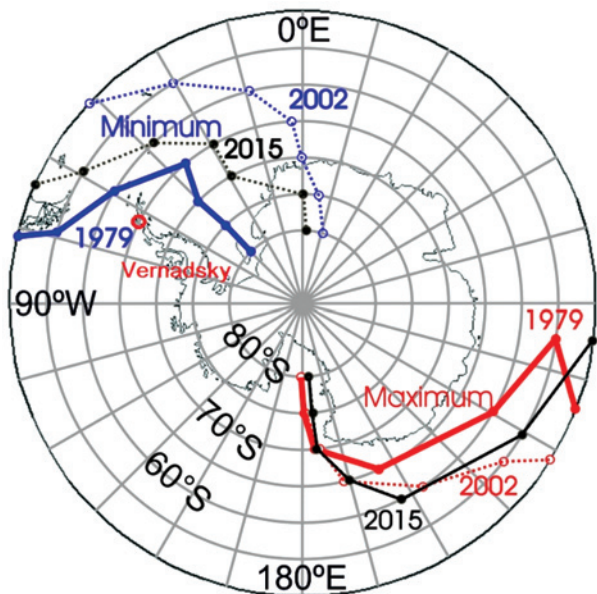


Figure 9. Map of longitudinal locations of zonal quasi-stationary planetary wave (QSW) maximum (red) and zonal QSW minimum (blue) at seven latitudes between 50 and 80°S; westernmost (easternmost) longitudes in 1979 (2002) determined from the polynomial fit, are shown by solid (dotted) lines. Black lines mark longitudes for 2015. Modified from (Siddaway et al., 2020)

Moreover, this effect was significant for ozone measurements taken inside/outside the polar vortex for stations in the vortex edge region (Hassler et al., 2011). For example, with the shifting of the ozone minimum to the east, further from the Faraday/Vernadsky station, a greater portion of the ozone measurements are located outside the vortex, where ozone values are higher. This suggests that dynamical influence must be considered when interpreting and intercomparing ozone measurements from Antarctic stations for detecting ozone recovery and ozone related changes in the Antarctic climate (Hassler et al., 2011).

Another important result was obtained in the teleconnection analysis between the tropics and the Antarctic stratosphere (Evtushevsky et al., 2015; 2019). Using the sequential formation of temperature variability indices method, it was possible to identify the tropical heat source and the region of maximum response to it in the western part of the stratosphere over Antarctica. The analysis consisted of 4 steps: (1) correlation of the generally accepted climate Niño 4

index for the temperature in the central part of the tropical Pacific with the temperature of the Antarctic stratosphere; it revealed a regional correlation maximum in the western stratosphere; (2) formation of the stratospheric temperature variability index in the segment of the maximum correlation and the next step of correlation of this index with the surface temperature (sea surface temperature – SST) in the tropical Pacific. The correlation maximum was found, which in latitudinal extent was four times greater than the area characterized by the Niño 4 index; a new SST index has been introduced for this area, an alternative to the Niño 4 index. Third step, (3) correlation of the SST index with the temperature field of the Antarctic stratosphere, which more accurately determined the spatial extent of the maximum regional response to the tropical source of thermal disturbances; (4) formation of the final temperature variability index in the western stratosphere over Antarctica and its correlation with the SST field; not only the geographical boundaries but also the shape of the tropical source in the Pacific Ocean (Fig. 4b), the so-called V-structure, were established.

The maximum teleconnection is found between thermal anomalies in the source region in June and temperature anomalies in the western stratosphere over Antarctica in October, with a delay of four months and with the penetration of the tropical signal into the troposphere (Evtushevsky et al., 2015; 2019). In this case, a methodological feature of the analysis was the consistent clarification of the geographical location and shape of the areas in maximum teleconnection and the determination of the structure of the planetary waves involved in this connection.

Unlike other works where teleconnection was studied in relation to the El Niño phase (e.g., Yang et al., 2015; Domeisen et al., 2019), the method used in (Evtushevsky et al., 2015; 2019) provides climatological patterns of coupled interannual variability of disturbances in remote regions. Described methods allow investigating the distribution of tropopause location, asymmetry, and anomalies (Evtushevsky et al., 2008b; 2011; Grytsai et al., 2008). The results of climatological tropopause anomalies study in polar

winter and spring and relationships to troposphere-stratosphere coupling in the polar atmosphere are presented in (Evtushevsky et al., 2011).

It is also worth noting the establishment of the effect of wave disturbances in the temperature distribution of the Antarctic stratosphere in August (at the end of winter in the southern hemisphere) on the state of the ozone hole in the spring months of September–November. A comparative analysis of the correlation ratios between the amplitude of PW in the temperature of the stratosphere in the winter months and the area of the ozone hole in the spring months showed that August anomalies of the amplitude give the greatest contribution to the interannual changes in the area of the ozone hole (Kravchenko et al., 2012; Milinevsky et al., 2020; Milinevsky et al., 2022). A predictive index was formed for the prerequisites for the development of the ozone hole, which showed high reliability in predicting an anomalous decrease in its area in 2017 and 2019 (Kravchenko et al., 2018; Milinevsky et al., 2020). As known, fairly reliable forecasts of the ozone hole state is possible on a synoptic timescale of 5–10 days (see e.g. forecasting service in the TEMIS project at <https://www.temis.nl/protocols/O3forecast.php>). Existing forecasts of stratospheric processes are less reliable on a seasonal scale. The identification of the factors that limit the seasonal predictability is an important problem in global climate forecasting (Tripathi et al., 2015) and there are a number of challenges exists and seasonal forecasting is expected to focus on in the near future (Doblas-Reyes et al., 2013; Wang et al., 2022).

The use of the analysis methods allowed specific atmospheric influences to be examined. This revealed changes in the spectral components of PWs at different phases of SSW (Wang et al., 2019; 2021; Shi et al., 2021; Zhang et al., 2022b), long-term trends in the zonal asymmetry of the Arctic stratopause (Shi et al., 2022), and significant differences in the annual cycle of ozone when considering the zonal asymmetry in the distribution of ozone associated with the structure of quasi-stationary PWs (Zhang et al., 2022a). The analyses also identified variations in mesospheric CO associated with geographical migrations of the edge of the displaced stratospheric polar vortex and its fragments (Wang et al., 2019).

Local microwave radiometer measurements of CO above Kharkiv, Ukraine (50.0°N , 36.3°E) in January–March 2018 were compared with the CO field and time–altitude sections of CO from the MLS data. Polar maps of CO at four pressure levels corresponding to altitudes of 32, 50, 75, and 86 km were considered. Replacement of the CO-rich polar vortex air by CO-poor air of the surrounding area led to a significant mesospheric CO decrease over the station during the SSW. Variations in the vertical CO profile showed that vortex fragmentation over the station at the SSW start caused episodic enhancement of stratospheric CO at about 30 km. This indicated penetration of the mesospheric CO levels into the middle stratosphere immediately after the SSW onset (Wang et al., 2019).

6 Conclusions

We discuss the methods of analysing the characteristics of planetary waves and the data sources used in this process. We describe the methods, data sources, and examples of planetary waves study in the framework of a collaborative study of Ukrainian, Chinese, and Australian researchers. The parameters of the main ozonometric instruments (Dobson spectrophotometer, TOMS and OMI satellite spectrometers, MLS satellite radiometer) and the capabilities of atmospheric and ozone reanalyses (NCEP–NCAR, MERRA-2, ERA-Interim, MSR, and MOD) are characterized.

The structure of the data and tools for their analysis in the NCEP–NCAR reanalysis are given in more detail, as their availability contributed to the rapid visualization of the data, their quantitative analysis, and the optimal choice of the type of graphical representation. This accelerated obtaining the necessary output and, as a result, significantly increased research productivity. The method of spectral analysis of data series and samples of the use are outlined. The method allows a comprehensive description of the behavior of the spectral components of planetary waves under the conditions of dynamic changes in Antarctic ozone in the winter-spring season.

The main examples of the data use and the application of analytical methods and their combinations in the study of the dynamics of the atmosphere under

the influence of PW and SSW published by authors are presented. A long-term shift of the TOC zonal minimum over the Antarctic to the East in the spring months with the largest PW activity in the Antarctic stratosphere was revealed (Grytsai et al., 2007; 2017). The spatial and temporal characteristics of the maximum teleconnection between the tropical heat source of atmospheric disturbances and the response to them in the western part of the Antarctic stratosphere were determined (Evtushevsky et al., 2015; 2019). A predictive index was created for the possible anomalous ozone hole development in the spring months (Kravchenko et al., 2012; 2018; Milinevsky et al., 2020; 2022). Changes in the spectral components of PW at different phases of SSW (Wang et al., 2021; Shi et al., 2021; Zhang et al., 2022b), changes in the zonal asymmetry of the Arctic stratopause (Shi et al., 2022), peculiarities of the annual ozone cycle when considering the zonal asymmetry in the distribution of ozone associated with the structure of quasi-stationary PWs (Zhang et al., 2022a) were established. The connection between local variations in the mesospheric carbon monoxide from ground measurements and migrations of the edge of the shifted stratospheric polar vortex and the position of its fragments above the ground station was found (Wang et al., 2019).

Author contributions. Conceptualization: O. E. and G. M.; methodology: O. E., G. M., A. G., O. I., and Yu. A.; data acquisition: O. E., O. I., A. K., and Y. S.; software: A. G., O. E., and O. I.; validation: O. E., A. G., A. K., and G. M.; investigation: A. G., O. E., A. K., G. M., Y. S., and O. I.; writing—original draft preparation: O. E., A. K., and G. M.; writing—review and editing: O. E., A. K., A. G., and G. M.; visualization: O. I., O. E., and A. G.; supervision: G. M.; project administration: G. M. and O. E. Each author contributed to the interpretation and discussion of the results and edited the manuscript.

Acknowledgments. This work was partially supported by the College of Physics, International Center of Future Science, Jilin University, China, and by the Ministry of Education and Science of Ukraine with the grant BF30-2021 at the Taras Shevchenko National University of Kyiv. This work contributed to

Project 4293 of the Australian Antarctic Program and the State Institution National Antarctic Scientific Center of Ukraine's research objectives. We thank observers at the Vernadsky and Kyiv-Goloseyev stations for total ozone data. We acknowledge the Goddard Earth Sciences Data and Information Services Center for TOC data from Total Ozone Mapping Spectrometer (Earth Probe) and the National Aeronautics and Space Administration, Goddard Space Flight Center for Ozone Monitoring Instrument and MLS (Aura) measurements (<https://disc.gsfc.nasa.gov/datasets/>, <https://ozonewatch.gsfc.nasa.gov/>). The Aura Microwave Limb Sounder (MLS) measurements were obtained from <https://mls.jpl.nasa.gov/data/readers.php>. The MERRA-2 data were obtained from https://acd-ext.gsfc.nasa.gov/Data_services/met/ann_data.html site. Data from the reanalysis are available on the NOAA website <https://psl.noaa.gov/data/gridded/data.ncep.reanalysis.html>. Authors thank two anonymous reviewers for the valuable comments and suggestions that helps to improve the paper significantly.

Funding. This research received no external funding.

Conflicts of Interest. The authors declare no conflict of interest.

References

- Agosta, E. A., & Canziani, P. O. (2010). Interannual variations in the zonal asymmetry of the subpolar latitudes total ozone column during the austral spring. *Geoacta*, 35(1), 1–16.
- Allen, D. R., Bevilacqua, R. M., Nedoluha, G. E., Randall, C. E., & Manney, G. L. (2003). Unusual stratospheric transport and mixing during the 2002 Antarctic winter. *Geophysical Research Letters*, 30(12), 1599. <https://doi.org/10.1029/2003GL017117>
- Angot, G., Keckhut, P., Hauchecorne, A., & Claud, C. (2012). Contribution of stratospheric warmings to temperature trends in the middle atmosphere from the lidar series obtained at Haute-Provence Observatory (44°N). *Journal of Geophysical Research: Atmospheres*, 117(D21), D21102. <https://doi.org/10.1029/2012JD017631>
- Antón, M., Koukouli, M. E., Kroon, M., McPeters, R. D., Labow, G. J., Balis, D., & Serrano, A. (2010). Global validation of empirically corrected EP-Total Ozone Mapping Spectrometer (TOMS) total ozone columns using Brewer and Dobson ground-based measurements. *Journal of Geophysical Research: Atmospheres*, 115(D19), D19305. <https://doi.org/10.1029/2010JD014178>

- Baldwin, M. P., & Dunkerton, T. J. (2001). Stratospheric harbingers of anomalous weather regimes. *Science*, 294(5542), 581–584. <https://doi.org/10.1126/science.1063315>
- Baldwin, M. P., Ayarzagüena, B., Birner, T., Butchart, N., Butler, A. H., Charlton-Perez, A. J., Domeisen, D. I. V., Garfinkel, C. I., Garny, H., Gerber, E. P., Hegglin, M. I., Langematz, U., & Pedatella, N. M. (2021). Sudden stratospheric warmings. *Reviews of Geophysics*, 59(1), e2020RG000708. <https://doi.org/10.1029/2020RG000708>
- Bramstedt, K., Gleason, J., Loyola, D., Thomas, W., Bracher, A., Weber, M., & Burrows, J. P. (2003). Comparison of total ozone from the satellite instruments GOME and TOMS with measurements from the Dobson network 1996–2000. *Atmospheric Chemistry and Physics*, 3(5), 1409–1419. <https://doi.org/10.5194/acp-3-1409-2003>
- Burrows, J. P., Weber, M., Buchwitz, M., Rozanov, V., Ladstätter-Weißenmayer, A., Richter, A., DeBeek, R., Hoogen, R., Bramstedt, K., Eichmann, K.-U., Eisinger, M., & Perner, D. (1999). The Global Ozone Monitoring Experiment (GOME): Mission Concept and First Scientific Results. *Journal of the Atmospheric Sciences*, 56(2), 151–175. [https://doi.org/10.1175/1520-0469\(1999\)056<056:TGOME>2.0.CO;2](https://doi.org/10.1175/1520-0469(1999)056<056:TGOME>2.0.CO;2)
- Butler, A. H., & Gerber, E. P. (2018). Optimizing the definition of a sudden stratospheric warming. *Journal of Climate*, 31(6), 2337–2344. <https://doi.org/10.1175/JCLI-D-17-0648.1>
- Butler, A. H., Sjoberg, J. P., Seidel, D. J., & Rosenlof, K. H. (2017). A sudden stratospheric warming compendium. *Earth System Science Data*, 9(1), 63–76. <https://doi.org/10.5194/essd-9-63-2017>
- Butler, A. H., Lawrence, Z. D., Lee, S. H., Lillo, S. P., & Long, C. S. (2020). Differences between the 2018 and 2019 stratospheric polar vortex split events. *Quarterly Journal of the Royal Meteorological Society*, 146 (732), 3503–3521. <https://doi.org/10.1002/qj.3858>
- Chandran, A., & Collins, R. L. (2014). Stratospheric sudden warming effects on winds and temperature in the middle atmosphere at middle and low latitudes: a study using WACCM. *Annales Geophysicae*, 32(7), 859–874. <https://doi.org/10.5194/angeo-32-859-2014>
- Chandran, A., Collins, R. L., Garcia, R. R., & Marsh, D. R. (2011). A case study of an elevated stratopause generated in the Whole Atmosphere Community Climate Model. *Geophysical Research Letters*, 38(8), L08804. <https://doi.org/10.1029/2010GL046566>
- Chandran, A., Collins, R. L., Garcia, R. R., Marsh, D. R., Harvey, V. L., Yue, J., & de la Torre, L. (2013). A climatology of elevated stratopause events in the whole atmosphere community climate model. *Journal of Geophysical Research: Atmospheres*, 118(3), 1234–1246. <https://doi.org/10.1002/jgrd.50123>
- Charlton, A. J., & Polvani, L. M. (2007). A new look at stratospheric sudden warmings. Part I: Climatology and modeling benchmarks. *Journal of Climate*, 20(3), 449–469. <https://doi.org/10.1175/JCLI3996.1>
- Choi, H., Kim, J.-H., Kim, B.-M., & Kim, S.-J. (2021). Observational evidence of distinguishable weather patterns for three types of sudden stratospheric warming during northern winter. *Frontiers in Earth Science*, 9, 625868. <https://doi.org/10.3389/feart.2021.625868>
- Chubachi, S. (1984). Preliminary result of ozone observations at Syowa station from February 1982 to January 1983. *Memoirs of National Institute of Polar Research Japan, Special issue*, 34, 13–19.
- Constantin, A. (2016). *Fourier Analysis (London Mathematical Society Student Texts). Volume 1: Theory*. Cambridge University Press. <https://doi.org/10.1017/CBO9781107358508>
- Curbelo, J., Chen, G., & Mechoso, C. R. (2021). Lagrangian analysis of the northern stratospheric polar vortex split in April 2020. *Geophysical Research Letters*, 48(16), e2021GL093874. <https://doi.org/10.1029/2021GL093874>
- Dee, D. P., Uppala, S. M., Simmons, A. J., Berrisford, P., Poli, P., Kobayashi, S., Andrae, U., Balmaseda, M. A., Balsamo, G., Bauer, P., Bechtold, P., Beljaars, A. C. M., van de Berg, L., Bidlot, J., Bormann, N., Delsol, C., Dragani, R., Fuentes, M., Geer, A. J., ... & Vitart, F. (2011). The ERA-Interim reanalysis: configuration and performance of the data assimilation system. *Quarterly Journal of the Royal Meteorological Society*, 137(656), Part A, 553–597. <https://doi.org/10.1002/qj.828>
- de la Torre, L., Garcia, R. R., Barriopedro, D., & Chandran, A. (2012). Climatology and characteristics of stratospheric sudden warmings in the Whole Atmosphere Community Climate Model. *Journal of Geophysical Research: Atmospheres*, 117(D4), D04110. <https://doi.org/10.1029/2011JD016840>
- de Wit, R. J., Hibbins, R. E., Espy, P. J., Orsolini, Y. J., Limpasuvan, V., & Kinnison, D. E. (2014). Observations of gravity wave forcing of the mesopause region during the January 2013 major Sudden Stratospheric Warming. *Geophysical Research Letters*, 41(13), 4745–4752. <https://doi.org/10.1002/2014GL060501>
- Dhomse, S. S., Kinnison, D., Chipperfield, M. P., Salawitch, R. J., Cionni, I., Hegglin, M. I., Abraham, N. L., Akiyoshi, H., Archibald, A. T., Bednarz, E. M., Bekki, S., Braesicke, P., Butchart, N., Dameris, M., Deushi, M., Frith, S., Hardiman, S. C., Hassler, B., Horowitz, L. W., ... & Zeng, G. (2018). Estimates of ozone return dates from Chemistry-Climate Model Initiative simulations. *Atmospheric Chemistry and Physics*, 18(11), 8409–8438. <https://doi.org/10.5194/acp-18-8409-2018>
- Di Biagio, C., Muscari, G., di Sarra, A., de Zafra, R. L., Eriksen, P., Fiocco, G., Fiorucci, I., & Fuà, D. (2010). Evolution of temperature, O₃, CO, and N₂O profiles during the exceptional 2009 Arctic major stratospheric warming as observed by lidar and millimeter-wave spectroscopy at Thule (76.5°N, 68.8°W), Greenland. *Journal of Geophysical Research: Atmospheres*, 115(D24), D24315. <https://doi.org/10.1029/2010JD014070>

- Doblas-Reyes, F. J., García-Serrano, J., Lienert, F., Biescas, A. P., & Rodrigues, L. R. L. (2013). Seasonal climate predictability and forecasting: status and prospects. *WIREs (Wiley Interdisciplinary Reviews) Climate Change*, 4(4), 245–268. <https://doi.org/10.1002/wcc.217>
- Domeisen, D. I. V., Garfinkel, C. I., & Butler, A. H. (2019). The teleconnection of El Niño Southern Oscillation to the stratosphere. *Reviews of Geophysics*, 57(1), 5–47. <https://doi.org/10.1029/2018RG000596>
- Domeisen, D. I. V., Grams, C. M., & Papritz, L. (2020). The role of North Atlantic–European weather regimes in the surface impact of sudden stratospheric warming events. *Weather and Climate Dynamics*, 1(2), 373–388. <https://doi.org/10.5194/wcd-1-373-2020>
- Dwyer, J. G., & O’Gorman, P. A. (2017). Moist formulations of the Eliassen–Palm flux and their connection to the surface westerlies. *Journal of the Atmospheric Sciences*, 74(2), 513–530. <https://doi.org/10.1175/JAS-D-16-0111.1>
- Evans, R. D. (2008). *Operations handbook – ozone observations with a Dobson spectrophotometer: Revised 2008*, GAW Report No. 183, WMO/TD-No. 1469.
- Evtushevsky, O., Milinevsky, G., Grytsai, A., Kravchenko, V., Grytsai, Z., & Leonov, M. (2008a). Comparison of ground-based Dobson and satellite EP-TOMS total ozone measurements over Vernadsky station, Antarctica, 1996–2005. *International Journal of Remote Sensing*, 29 (9), 2675–2683. <https://doi.org/10.1080/01431160701767591>
- Evtushevsky, O. M., Grytsai, A. V., Klekociuk, A. R., & Milinevsky, G. P. (2008b). Total ozone and tropopause zonal asymmetry during the Antarctic spring. *Journal of Geophysical Research: Atmospheres*, 113(D7), D00B06. <https://doi.org/10.1029/2008JD009881>
- Evtushevsky, O., Klekociuk, A., Grytsai, A., Milinevsky, G., & Lozitsky, V. (2011). Troposphere and stratosphere influence on tropopause in the polar regions during winter and spring. *International Journal of Remote Sensing*, 32(11), 3153–3164. <http://dx.doi.org/10.1080/01431161.2010.541515>
- Evtushevsky, O. M., Kravchenko, V. O., Hood, L. L., & Milinevsky, G. P. (2015). Teleconnection between the central tropical Pacific and the Antarctic stratosphere: spatial patterns and time lags. *Climate Dynamics*, 44, 1841–1855. <https://doi.org/10.1007/s00382-014-2375-2>
- Evtushevsky, O. M., Grytsai, A. V., & Milinevsky, G. P. (2019). Decadal changes in the central tropical Pacific teleconnection to the Southern Hemisphere extratropics. *Climate Dynamics*, 52, 4027–4055. <https://doi.org/10.1007/s00382-018-4354-5>
- Eyring, V., Bony, S., Meehl, G. A., Senior, C. A., Stevens, B., Stouffer, R. J., & Taylor, K. E. (2016). Overview of the Coupled Model Intercomparison Project Phase 6 (CMIP6) experimental design and organization. *Geoscientific Model Development*, 9(5), 1937–1958. <https://doi.org/10.5194/gmd-9-1937-2016>
- Farman, J. C., Gardiner, B. G., & Shanklin, J. D. (1985). Large losses of total ozone in Antarctica reveal seasonal ClO_x/NO_x interaction. *Nature*, 315, 207–210. <https://doi.org/10.1038/315207a0>
- Fleming, E. L., Chandra, S., Barnett, J. J., & Corney, M. (1990). Zonal mean temperature, pressure, zonal wind and geopotential height as functions of latitude. *Advances in Space Research*, 10(12), 11–59. [https://doi.org/10.1016/0273-1177\(90\)90386-E](https://doi.org/10.1016/0273-1177(90)90386-E)
- Flynn, L., Long, C., Wu, X., Evans, R., Beck, C. T., Petropavlovskikh, I., McConville, G., Yu, W., Zhang, Z., Niu, J., Beach, E., Hao, Y., Pan, C., Sen, B., Novicki, M., Zhou, S., & Seftor, C. (2014). Performance of the Ozone Mapping and Profiler Suite (OMPS) products. *Journal of Geophysical Research: Atmospheres*, 119(10), 6181–6195. <https://doi.org/10.1002/2013JD020467>
- Forkman, P., Christensen, O. M., Eriksson, P., Billade, B., Vassilev, V., & Shulga, V. M. (2016). A compact receiver system for simultaneous measurements of mesospheric CO and O₃. *Geoscientific Instrumentation, Methods and Data Systems* 5(1), 27–44. <https://doi.org/10.5194/gi-5-27-2016>
- France, J. A., & Harvey, V. L. (2013). A climatology of the stratopause in WACCM and the zonally asymmetric elevated stratopause. *Journal of Geophysical Research: Atmospheres*, 118(5), 2241–2254. <https://doi.org/10.1002/jgrd.50218>
- Friedel, M., Chiodo, G., Stenke, A., Domeisen, D. I. V., Fueglistaler, S., Anet, J. G., & Peter, T. (2022). Springtime arctic ozone depletion forces northern hemisphere climate anomalies. *Nature Geoscience*, 15, 541–547. <https://doi.org/10.1038/s41561-022-00974-7>
- Frith, S. M., Kramarova, N. A., Stolarski, R. S., McPeters, R. D., Bhartia, P. K., & Labow, G. J. (2014). Recent changes in total column ozone based on the SBUV Version 8.6 Merged Ozone Data Set. *Journal of Geophysical Research: Atmospheres*, 119(16), 9735–9751. <https://doi.org/10.1002/2014JD021889>
- Funke, B., López-Puertas, M., García-Comas, M., Stiller, G. P., von Clarmann, T., Höpfner, M., Glatthor, N., Grabowski, U., Kellmann, S., & Linden, A. (2009). Carbon monoxide distributions from the upper troposphere to the mesosphere inferred from 4.7 μm non-local thermal equilibrium emissions measured by MIPAS on Envisat. *Atmospheric Chemistry and Physics*, 9(7), 2387–2411. <https://doi.org/10.5194/acp-9-2387-2009>
- Gardner, C. S. (2018). Role of wave-induced diffusion and energy flux in the vertical transport of atmospheric constituents in the mesopause region. *Journal of Geophysical Research: Atmospheres*, 123(12), 6581–6604. <https://doi.org/10.1029/2018JD028359>
- Garcelon, R., McCarty, W., Suárez, M. J., Todling, R., Molod, A., Takacs, L., Randles, C. A., Darmenov, A., Bosilovich, M. G., Reichle, R., Wargan, K., Coy, L., Cullather, R., Draper, C., Akella, S., Buchard, V., Conaty, A., da Silva, A. M., Gu, W., ... & Zhao, B. (2017). The Modern-Era Retrospective Analysis for Research and Applications, Version 2 (MERRA-2).

- Journal of Climate*, 30(14), 5419–5454. <https://doi.org/10.1175/jcli-d-16-0758.1>
- Godin-Beekmann, S. (2010). Spatial observation of the ozone layer. *Comptes Rendus Geoscience*, 342(4–5), 339–348. <https://doi.org/10.1016/j.crte.2009.10.012>
- Gritsai, Z. I., Evtushevsky, A. M., Leonov, N. A., & Milinevsky, G. P. (2000). Comparison of ground-based TOMS-EP total ozone data for Antarctica and northern midlatitude stations (1996–1999). *Physics and Chemistry of the Earth. Part B: Hydrology, Oceans and Atmosphere*, 25(5–6), 459–461. [https://doi.org/10.1016/S1464-1909\(00\)00044-7](https://doi.org/10.1016/S1464-1909(00)00044-7)
- Grytsai, A. (2011). Planetary wave peculiarities in Antarctic ozone distribution during 1979–2008. *International Journal of Remote Sensing*, 32(11), 3139–3151. <https://doi.org/10.1080/01431161.2010.541518>
- Grytsai, A. & Milinevsky, G. (2013). SCIAMACHY/EnviroSat, OMI/Aura, and ground-based total ozone measurements over Kyiv-Goloseyev station. *International Journal of Remote Sensing*, 34(15), 5611–5622. <http://dx.doi.org/10.1080/01431161.2013.794988>
- Grytsai, A., Grytsai, Z., Evtushevsky, A., & Milinevsky, G. (2005a). Interannual variability of planetary waves in the ozone layer at 65°S. *International Journal of Remote Sensing*, 26(16), 3377–3387. <https://doi.org/10.1080/01431160500076350>
- Grytsai, A., Grytsai, Z., Evtushevsky, A., Milinevsky, G., & Leonov, N. (2005b). Zonal wave numbers 1–5 in planetary waves from the TOMS total ozone at 65°S. *Annales Geophysicae*, 23(5), 1565–1573. <https://doi.org/10.5194/angeo-23-1565-2005>
- Grytsai, A. V., Evtushevsky, O. M., Milinevsky, G. P., Grytsai, Z. I., & Agapitov, O. V. (2005c). Longitudinal distribution of total ozone content in edge region of antarctic stratospheric vortex. *Space Science and Technology*, 11(5–6). <https://doi.org/10.15407/knit2005.05.005>
- Grytsai, A. V., Evtushevsky, O. M., Agapitov, O. V., Klekociuk, A. R., & Milinevsky, G. P. (2007). Structure and long-term change in the zonal asymmetry in Antarctic total ozone during spring. *Annales Geophysicae*, 25(2), 361–374. <https://doi.org/10.5194/angeo-25-361-2007>
- Grytsai, A. V., Evtushevsky, O. M., & Milinevsky, G. P. (2008). Anomalous quasi-stationary planetary waves over the Antarctic region in 1988 and 2002. *Annales Geophysicae*, 26(5), 1101–1108. <https://doi.org/10.5194/angeo-26-1101-2008>
- Grytsai, A., Klekociuk, A., Milinevsky, G., Evtushevsky, O., & Stone, K. (2017). Evolution of the eastward shift in the quasi-stationary minimum of the Antarctic total ozone column. *Atmospheric Chemistry and Physics*, 17(3), 1741–1758. <https://doi.org/10.5194/acp-17-1741-2017>
- Grytsai, A., Milinevsky, G., Andrienko, Yu., Klekociuk, A., Rapoport, Yu., & Ivaniha, O. (2022). Antarctic planetary wave spectrum under different polar vortex conditions in 2019 and 2020 based on total ozone column data. *Ukrainian Antarctic Journal*, 20(1), 31–43. <https://doi.org/10.33275/1727-7485.1.2022.687>
- Hassler, B., Bodeker, G. E., Solomon, S., & Young, P. J. (2011). Changes in the polar vortex: Effects on Antarctic total ozone observations at various stations. *Geophysical Research Letters*, 38(1), L01805. <https://doi.org/10.1029/2010GL045542>
- Hersbach, H., Bell, B., Berrisford, P., Hirahara, S., Horányi, A., Muñoz-Sabater, J., Nicolas, J., Peubey, C., Radu, R., Schepers, D., Simmons, A., Soci, C., Abdalla, S., Abellán, X., Balsamo, G., Bechtold, P., Biavati, G., Bidlot, J., Bonavita, M., ... & Thépaut, J.-N. (2020). The ERA5 global reanalysis. *Quarterly Journal of the Royal Meteorological Society*, 146(730), 1999–2049. <https://doi.org/10.1002/qj.3803>
- Hoffmann, C. G., Raffalski, U., Palm, M., Funke, B., Golchert, S. H. W., Hochschild, G., & Notholt, J. (2011). Observation of strato-mesospheric CO above Kiruna with ground-based microwave radiometry—retrieval and satellite comparison. *Atmospheric Measurement Techniques*, 4(11), 2389–2408. <https://doi.org/10.5194/amt-4-2389-2011>
- Hongming, Y., Yuan, Y., Guirong, T., & Yucheng, Z. (2022). Possible impact of sudden stratospheric warming on the intraseasonal reversal of the temperature over East Asia in winter 2020/21. *Atmospheric Research*, 268, 106016. <https://doi.org/10.1016/j.atmosres.2022.106016>
- Hu, J., Ren, R., & Xu, H. (2014). Occurrence of winter stratospheric sudden warming events and the seasonal timing of spring stratospheric final warming. *Journal of the Atmospheric Sciences*, 71(7), 2319–2334. <https://doi.org/10.1175/JAS-D-13-0349.1>
- Hu, D., Tian, W., Xie, F., Wang, C., & Zhang, J. (2015). Impacts of stratospheric ozone depletion and recovery on wave propagation in the boreal winter stratosphere. *Journal of Geophysical Research: Atmospheres*, 120(16), 8299–8317. <https://doi.org/10.1002/2014JD022855>
- Huck, P. E., McDonald, A. J., Bodeker, G. E., & Struthers, H. (2005). Interannual variability in Antarctic ozone depletion controlled by planetary waves and polar temperature. *Geophysical Research Letters*, 32(13), L13819. <https://doi.org/10.1029/2005GL022943>
- Huret, N., Pirre, M., Hauchecorne, A., Robert, C., & Catoire, V. (2006). On the vertical structure of the stratosphere at midlatitudes during the first stage of the polar vortex formation and in the polar region in the presence of a large mesospheric descent. *Journal of Geophysical Research: Atmospheres*, 111(D6), D06111. <https://doi.org/10.1029/2005JD006102>
- Ivaniha, O. (2020). Long-term analysis of the Antarctic total ozone zonal asymmetry by MERRA-2 and CMIP6 data. *Ukrainian Antarctic Journal*, 1, 41–55. <https://doi.org/10.33275/1727-7485.1.2020.378>
- Kalnay, E., Kanamitsu, M., Kistler, R., Collins, W., Deaven, D., Gandin, L., Iredell, M., Saha, S., White, G., Woollen, J., Zhu, Y., Chelliah, M., Ebisuzaki, W., Higgins, W., Janowiak, J., Mo, K. C., Ropelewski, C., Wang, J., Leetmaa, A., ... & Joseph, D. (1996). The NCEP–NCAR 40-year reanalysis project. *Bulletin of the American Meteorological Society*, 77(3),

- 437–472. [https://doi.org/10.1175/1520-0477\(1996\)077<0437:TNYRP>2.0.CO;2](https://doi.org/10.1175/1520-0477(1996)077<0437:TNYRP>2.0.CO;2)
- Karpechko, A. Yu., Charlton-Perez, A., Balmaseda, M., Tyrrell, N., & Vitart, F. (2018). Predicting sudden stratospheric warming 2018 and its climate impacts with a multimodel ensemble. *Geophysical Research Letters*, 45(24), 13538–13546. <https://doi.org/10.1029/2018GL081091>
- Keller, J. D., & Wahl, S. (2021). Representation of climate in reanalyses: An intercomparison for Europe and North America. *Journal of Climate*, 34(5), 1667–1684. <https://doi.org/10.1175/JCLI-D-20-0609.1>
- Kistler, R., Kalnay, E., Collins, W., Saha, S., White, G., Woollen, J., Chelliah, M., Ebisuzaki, W., Kanamitsu, M., Kousky, V., van der Dool, H., Jenne, R., & Fiorino, M. (2001). The NCEP–NCAR 50-Year Reanalysis: Monthly Means CD-ROM and Documentation. *Bulletin of the American Meteorological Society*, 82(2), 247–268. [https://doi.org/10.1175/1520-0477\(2001\)082<0247:tnnyrm>2.3.co;2](https://doi.org/10.1175/1520-0477(2001)082<0247:tnnyrm>2.3.co;2)
- Kodera, K., Mukougawa, H., Maury, P., Ueda, M., & Claud, C. (2016). Absorbing and reflecting sudden stratospheric warming events and their relationship with tropospheric circulation. *Journal of Geophysical Research: Atmospheres*, 121(1), 80–94. <https://doi.org/10.1002/2015JD023359>
- Kravchenko, V., Evtushevsky, A., Grytsai, A., Milinevsky G., & Shanklin, J. (2009). Total ozone dependence of the difference between the empirically corrected EP-TOMS and high-latitude station datasets. *International Journal of Remote Sensing*, 30(15–16), 4283–4294. <https://doi.org/10.1080/01431160902825008>
- Kravchenko, V. O., Evtushevsky, O. M., Grytsai, A. V., Klekociuk, A. R., Milinevsky, G. P., & Grytsai, Z. I. (2012). Quasi-stationary Planetary Waves in Late Winter Antarctic Stratosphere Temperature as a Possible Indicator of Spring Total Ozone. *Atmospheric Chemistry and Physics*, 12(6), 2865–2879. <https://doi.org/10.5194/acp-12-2865-2012>
- Kravchenko, V. O., Evtushevsky, O. M., Grytsai, A. V., Milinevsky, G. P., & Klekociuk, A. R. (2018). Preconditions for the ozone hole decrease in 2017. *Ukrainian Journal of Remote Sensing*, 18, 5358. <https://doi.org/10.36023/ujrs.2018.18.130>
- Kvissel, O. K., Orsolini, Y. J., Stordal, F., Limpasuvan, V., Richter, J., & Marsh, D. R. (2012). Mesospheric intrusion and anomalous chemistry during and after a major stratospheric sudden warming. *Journal of Atmospheric and Solar-Terrestrial Physics*, 78–79, 116–124. <https://doi.org/10.1016/j.jastp.2011.08.015>
- Lee, S. H., & Butler, A. H. (2020). The 2018–2019 Arctic stratospheric polar vortex. *Weather*, 75(2), 52–57. <https://doi.org/10.1002/wea.3643>
- Levett, P. F., Hilsenrath, E., Leppelmeier, G. W., van den Oord, G. H. J., Bhartia, P. K., Tamminen, J., de Haan, J. F., & Veefkind, J. P. (2006). Science objectives of the ozone monitoring instrument. *IEEE Transactions on Geoscience and Remote Sensing*, 44(5), 1199–1208. <https://doi.org/10.1109/TGRS.2006.872336>
- Limpasuvan, V., Orsolini, Y. J., Chandran, A., Garcia, R. R., & Smith, A. K. (2016). On the composite response of the MLT to major sudden stratospheric warming events with elevated stratopause. *Journal of Geophysical Research: Atmospheres*, 121(9), 4518–4537. <https://doi.org/10.1002/2015JD024401>
- Lin, P., Fu, Q., Solomon, S., & Wallace, J. M. (2009). Temperature trend patterns in Southern Hemisphere high latitudes: Novel indicators of stratospheric change. *Journal of Climate*, 22(23), 6325–6341. <https://doi.org/10.1175/2009JCLI2971.1>
- Liu, G., Hirooka, T., Eguchi, N., & Krüger, K. (2022). Dynamical evolution of a minor sudden stratospheric warming in the Southern Hemisphere in 2019. *Atmospheric Chemistry and Physics*, 22(5), 3493–3505. <https://doi.org/10.5194/acp-22-3493-2022>
- Livingston, N. J., Read, W. G., Wagner, P. A., Froidevaux, L., Santee, M. L., Schwartz, M. J., Lambert, A., Millán Valle, L. F., Pumphrey, H. C., Manney, G. L., Fuller, R. A., Jarnot, R. F., Knosp, B. W., & Lay, R. R. (2022). *Earth Observing System (EOS) Aura Microwave Limb Sounder (MLS) version 5.0x Level 2 and 3 data quality and description document. Version 5.0x–1.1a* (JPL D-105336 Rev. B.). Jet Propulsion Laboratory, California Institute of Technology. https://mls.jpl.nasa.gov/data/v5-0_data_quality_document.pdf
- Manney, G. L., Schwartz, M. J., Krüger, K., Santee, M. L., Pawson, S., Lee, J. N., Daffer, W. H., Fuller, R. A., & Livingstone, N. J. (2009). Aura Microwave Limb Sounder observations of dynamics and transport during the record-breaking 2009 Arctic stratospheric major warming. *Geophysical Research Letters*, 36(12), L12815. <https://doi.org/10.1029/2009GL038586>
- Manney, G. L., Lawrence, Z. D., Santee, M. L., Livingstone, N. J., Lambert, A., & Pitts, M. C. (2015). Polar processing in a split vortex: Arctic ozone loss in early winter 2012/2013. *Atmospheric Chemistry and Physics*, 15(10), 5381–5403. <https://doi.org/10.5194/acp-15-5381-2015>
- McPeters, R. D., Bhartia, P. K., Krueger, A. J., Herman, J. R., Wellemeyer, C. G., Seftor, C. J., Jaross, G., Torres, O., Moy, L., Labow, G., Byerly, W., Taylor, S. L., Swissler, T., & Cebula, R. P. (1998). *Earth Probe Total Ozone Mapping Spectrometer (TOMS) Data Products User's Guide* (NASA Technical Publication 1998-206895). National Aeronautics and Space Administration. Goddard Space Flight Center Greenbelt, Maryland.
- McPeters, R., Kroon, M., Labow, G., Brinksma, E., Balis, D., Petropavlovskikh, I., Veefkind, J. P., Bhartia, P. K., & Levitt, P. F. (2008). Validation of the Aura Ozone Monitoring Instrument total column ozone product. *Journal of Geophysical Research: Atmospheres*, 113(D15), D15S14. <https://doi.org/10.1029/2007JD008802>
- Milinevsky, G. P., Danylevsky, V. O., Grytsai, A. V., Evtushevsky, O. M., Kravchenko, V. O., Bovchaliuk, A. P., Bovchaliuk, V. P., Sosonkin, M. G., Goloub, Ph., Savitska, L. Y., Udodov, E. V., & Voytenko, V. P. (2012). Recent developments of atmospheric research in Ukraine. *Advances in Astronomy and Space Physics*, 2(2), 114–120.

- Milinevsky, G., Evtushevsky, O., Klekociuk, A., Wang, Y., Grytsai, A., Shulga, V., & Ivaniha, O. (2020). Early indications of anomalous behaviour in the 2019 spring ozone hole over Antarctica. *International Journal of Remote Sensing*, 41(19), 7530–7540. <https://doi.org/10.1080/2150704X.2020.1763497>
- Milinevsky, G. P., Grytsai, A. V., Evtushevsky, O. M., & Klekociuk, A. R. (2022). Contributions to understanding climate interactions: stratospheric ozone. Akademperiodyka. <https://doi.org/10.15407/academperiodyka.252.471>
- Orsolini, Y. J., Limpasuvan, V., Pérot, K., Espy, P., Hibbins, R., Lossow, S., Larsson, K. R., & Murtagh, D. (2017). Modelling the descent of nitric oxide during the elevated stratopause event of January 2013. *Journal of Atmospheric and Solar-Terrestrial Physics*, 155, 50–61. <https://doi.org/10.1016/j.jastp.2017.01.006>
- Pinsky, M. A. (2009). *Introduction to Fourier analysis and wavelets*. American Mathematical Society. <http://dx.doi.org/10.1090/gsm/102>
- Piters, A. J. M., Bramstedt, K., Lambert, J.-C., & Kirchhoff, B. (2006). Overview of SCIAMACHY validation: 2002–2004. *Atmospheric Chemistry and Physics*, 6, 127–148. <https://doi.org/10.5194/acp-6-127-2006>
- Randel, W. J., Wu, F., & Stolarski, R. (2002). Changes in column ozone correlated with the stratospheric EP flux. *Journal of the Meteorological Society of Japan. Ser. II*, 80(4B), 849–862. <https://doi.org/10.2151/jmsj.80.849>
- Rao, J., Ren, R., Chen, H., Yu, Y., & Zhou, Y. (2018). The stratospheric sudden warming event in February 2018 and its prediction by a climate system model. *Journal of Geophysical Research: Atmospheres*, 123(23), 13332–13345. <https://doi.org/10.1029/2018JD028908>
- Rüfenacht, R., Kämpfer, N., & Murk, A. (2012). First middle-atmospheric zonal wind profile measurements with a new ground-based microwave Doppler-spectro-radiometer. *Atmospheric Measurement Techniques*, 5(11), 2647–2659. <https://doi.org/10.5194/amt-5-2647-2012>
- Ryan, N. J., Kinnison, D. E., Garcia, R. R., Hoffmann, C. G., Palm, M., Raffalski, U., & Notholt, J. (2018). Assessing the ability to derive rates of polar middle-atmospheric descent using trace gas measurements from remote sensors. *Atmospheric Chemistry and Physics*, 18(3), 1457–1474. <https://doi.org/10.5194/acp-18-1457-2018>
- Salby, M. L. (1982). Sampling theory for synoptic satellite observations. Part II: Fast fourier synoptic mapping. *Journal of the Atmospheric Sciences*, 39(11), 2601–2614. [https://doi.org/10.1175/1520-0469\(1982\)039<2601:STFASO>2.0.CO;2](https://doi.org/10.1175/1520-0469(1982)039<2601:STFASO>2.0.CO;2)
- Salby, M. L., Titova, E. A., & Deschamps, L. (2012). Changes of the Antarctic ozone hole: controlling mechanisms, seasonal predictability, and evolution. *Journal of Geophysical Research: Atmospheres*, 117(D10), D10111. <https://doi.org/10.1029/2011JD016285>
- Salmi, S.-M., Verronen, P. T., Thölix, L., Kyrölä, E., Backman, L., Karpechko, A. Yu., & Seppälä, A. (2011). Mesosphere-to-stratosphere descent of odd nitrogen in February–March 2009 after sudden stratospheric warming. *Atmospheric Chemistry and Physics*, 11(10), 4645–4655. <https://doi.org/10.5194/acp-11-4645-2011>
- Scheffler, J., Ayarzagüena, B., Orsolini, Y. J., & Langematz, U. (2022). Elevated stratopause events in the current and a future climate: A chemistry-climate model study. *Journal of Atmospheric and Solar-Terrestrial Physics*, 227, 105804. <https://doi.org/10.1016/j.jastp.2021.105804>
- Schoeberl, M. R. (1978). Stratospheric warmings: Observations and theory. *Reviews of Geophysics*, 16(4), 521–538. <https://doi.org/10.1029/RG016i004p00521>
- Shi, Y., Evtushevsky, O., Shulga, V., Milinevsky, G., Klekociuk, A., Andrienko, Y., & Han, W. (2021). Mid-latitude mesospheric zonal wave 1 and wave 2 in recent boreal winters. *Remote Sensing*, 13(18), 3749. <https://doi.org/10.3390/rs13183749>
- Shi, Y., Evtushevsky, O., Milinevsky, G., Klekociuk, A., Han, W., Ivaniha, O., Andrienko, Y., Shulga, V., & Zhang, C. (2022). Zonal Asymmetry of the Stratopause in the 2019/2020 Arctic Winter. *Remote Sensing*, 14(6), 1496. <https://doi.org/10.3390/rs14061496>
- Shi, Y., Shulga, V., Ivaniha, O., Wang, Y., Evtushevsky, O., Milinevsky, G., Klekociuk, A., Patoka, A., Han, W., & Shulga, D. (2020). Comparison of major sudden stratospheric warming impacts on the mid-latitude mesosphere based on local microwave radiometer CO observations in 2018 and 2019. *Remote Sensing*, 12(23), 3950. <https://doi.org/10.3390/rs12233950>
- Siddaway, J., Klekociuk, A., Alexander, S. P., Grytsai, A., Milinevsky, G., Dargaville, R., Ivaniha, O., & Evtushevsky, O. (2020). Assessment of the zonal asymmetry trend in Antarctic total ozone column using TOMS measurements and CCM-Val-2 models. *Ukrainian Antarctic Journal*, 2, 50–58. <https://doi.org/10.33275/1727-7485.2.2020.652>
- Slivinski, L. C., Compo, G. P., Sardeshmukh, P. D., Whitaker, J. S., McColl, C., Allan, R. J., Brohan, P., Yin, X., Smith, C. A., Spencer, L. J., Vose, R. S., Rohrer, M., Conroy, R. P., Schuster, D. C., Kennedy, J. J., Ashcroft, L., Brönnimann, S., Brunet, M., Camuffo, D., ... & Wyszyński, P. (2021). An evaluation of the performance of the Twentieth Century Reanalysis Version 3. *Journal of Climate*, 34(4), 1417–1438. <https://doi.org/10.1175/JCLI-D-20-0505.1>
- Solomon, S. (1999). Stratospheric ozone depletion: A review of concepts and history. *Reviews of Geophysics*, 37(3), 275–316. <https://doi.org/10.1029/1999RG900008>
- Solomon, S., Garcia, R. R., Olivero, J. J., Bevilacqua, R. M., Schwartz, P. R., Clancy, R. T., & Muhleman, D. O. (1985). Photochemistry and transport of carbon monoxide in the middle atmosphere. *Journal of the Atmospheric Sciences*, 42(10), 1072–1083. [https://doi.org/10.1175/1520-0469\(1985\)042<1072:PATOCM>2.0.CO;2](https://doi.org/10.1175/1520-0469(1985)042<1072:PATOCM>2.0.CO;2)
- Solomon, S., Ivy, D. J., Kinnison, D., Mills, M. J., Neely III, R. R., & Schmidt, A. (2016). Emergence of healing in the Antarctic ozone layer. *Science*, 353(6296), 269–274. <https://doi.org/10.1126/science.aae0061>

- Staehelin, J., Petropavlovskikh, I., De Mazière, M., & Godin-Beekmann, S. (2018). The role and performance of ground-based networks in tracking the evolution of the ozone layer. *Comptes Rendus Geoscience*, 350(7), 354–367. <https://doi.org/10.1016/j.crte.2018.08.007>
- Taguchi, M. (2018). Comparison of subseasonal-to-seasonal model forecasts for major stratospheric sudden warmings. *Journal of Geophysical Research: Atmospheres*, 123(18), 10231–10247. <https://doi.org/10.1029/2018jd028755>
- Tanaka, D., Iwasaki, T., Uno, S., Ujiie, M., & Miyazaki, K. (2004). Eliassen–Palm flux diagnosis based on isentropic representation. *Journal of the Atmospheric Sciences*, 61(19), 2370–2383. [https://doi.org/10.1175/1520-0469\(2004\)061<2370:EFDBOI>2.0.CO;2](https://doi.org/10.1175/1520-0469(2004)061<2370:EFDBOI>2.0.CO;2)
- Tao, M., Konopka, P., Ploeger, F., Grooß, J.-U., Müller, R., Volk, C. M., Walker, K. A., & Riese, M. (2015). Impact of the 2009 major sudden stratospheric warming on the composition of the stratosphere. *Atmospheric Chemistry and Physics*, 15(15), 8695–8715. <https://doi.org/10.5194/acp-15-8695-2015>
- Teng, H., & Branstator, G. (2012). A zonal wave number 3 pattern of northern hemisphere wintertime planetary wave variability at high latitudes. *Journal of Climate*, 25(19), 6756–6769. <https://doi.org/10.1175/JCLI-D-11-00664.1>
- Tripathi, O. P., Baldwin, M., Charlton-Perez, A., Charron, M., Cheung, J. C. H., Eckermann, S. D., Gerber, E., Jackson, D. R., Kuroda, Yu., Lang, A., McLay, J., Mizuta, R., Reynolds, C., Roff, G., Sigmond, M., Son, S.-W., & Stockdale, T. (2016). Examining the predictability of the stratospheric sudden warming of January 2013 using multiple NWP systems. *Monthly Weather Review*, 144(5), 1935–1960. <https://doi.org/10.1175/mwr-d-15-0010.1>
- Tripathi, O. P., Baldwin, M., Charlton-Perez, A., Charron, M., Eckermann, S. D., Gerber, E., Harrison, R. G., Jackson, D. R., Kim, B.-M., Kuroda, Y., Lang, A., Mahmood, S., Mizuta, R., Roff, G., Sigmond, M., & Son, S.-W. (2015). The predictability of the extratropical stratosphere on monthly time-scales and its impact on the skill of tropospheric forecasts. *Quarterly Journal of the Royal Meteorological Society. Part B*, 141(689), 987–1003. <https://doi.org/10.1002/qj.2432>
- van der A, R. J., Allaart, M. A. F., & Eskes, H. J. (2010). Multi sensor reanalysis of total ozone. *Atmospheric Chemistry and Physics*, 10(22), 11277–11294. <https://doi.org/10.5194/acp-10-11277-2010>
- Wang, Y., Shulga, V., Milinevsky, G., Patoka, A., Evtushhevsky, O., Klekociuk, A., Han, W., Grytsai, A., Shulga, D., Myshenko, V., & Antyufeyev, O. (2019). Winter 2018 major sudden stratospheric warming impact on midlatitude mesosphere from microwave radiometer measurements. *Atmospheric Chemistry and Physics*, 19(15), 10303–10317. <https://doi.org/10.5194/acp-19-10303-2019>
- Wang, Y., Milinevsky, G., Evtushhevsky, O., Klekociuk, A., Han, W., Grytsai, A., Antyufeyev, O., Shi, Y., Ivaniha, O., & Shulga, V. (2021). Planetary wave spectrum in the stratosphere–mesosphere during sudden stratospheric warming 2018. *Remote Sensing*, 13(6), 1190. <https://doi.org/10.3390/rs13061190>
- Wang, H., Dai, Y., Yang, S., Li, T., Luo, J., Sun, B., Duan, M., Ma, J., Yin, Z., & Huang, Y. (2022). Predicting climate anomalies: A real challenge. *Atmospheric and Oceanic Science Letters*, 15(1), 100115. <https://doi.org/10.1016/j.aosl.2021.100115>
- Waters, J. W., Froidevaux, L., Harwood, R. S., Jarnot, R. F., Pickett, H. M., Read, W. G., Siegel, P. H., Cofield, R. E., Filipiak, M. J., Flower, D. A., Holden, J. R., Lau, G. K., Livesey, N. J., Manney, G. L., Pumphrey, H. C., Santee, M. L., Wu, D. L., Cuddy, D. T., Lay, R. R., ... & Walch, M. J. (2006). The Earth observing system microwave limb sounder (EOS MLS) on the Aura satellite. *IEEE Transactions on Geoscience and Remote Sensing*, 44(5), 1075–1092. <https://doi.org/10.1109/TGRS.2006.873771>
- Wirth, V. (1993). Quasi-stationary planetary waves in total ozone and their correlation with lower stratospheric temperature. *Journal of Geophysical Research: Atmospheres*, 98(D5), 8873–8882. <https://doi.org/10.1029/92JD02820>
- WMO (World Meteorological Organization). (2018). *Scientific Assessment of Ozone Depletion: 2018 (Global Ozone Research and Monitoring Project – Report No. 58)*.
- WMO (World Meteorological Organization). (2022). *Centennial observing stations: State of recognition Report – 2021 WMO-No. 1296 [Brochure]*. https://library.wmo.int/index.php?lvl=notice_display&id=22119#Y-Ikyy_P3IU
- Yang, C., Li, T., Dou, X., & Xue, X. (2015). Signal of central Pacific El Niño in the Southern Hemispheric stratosphere during austral spring. *Journal of Geophysical Research: Atmospheres*, 120(22), 11438–11450. <https://doi.org/10.1002/2015JD023486>
- Yu, Y., Cai, M., Shi, C., & Ren, R. (2018). On the linkage among strong stratospheric mass circulation, stratospheric sudden warming, and cold weather events. *Monthly Weather Review*, 146(9), 2717–2739. <https://doi.org/10.1175/MWR-D-18-0110.1>
- Zhang, C., Evtushevsky, O., Milinevsky, G., Klekociuk, A., Andrienko, Yu., Shulga, V., Han, W., & Shi, Y. (2022a). The annual cycle in mid-latitude stratospheric and mesospheric ozone associated with quasi-stationary wave structure by the MLS data 2011–2020. *Remote Sensing*, 14(10), 2309. <https://doi.org/10.3390/rs14102309>
- Zhang, C., Grytsai, A., Evtushevsky, O., Milinevsky, G., Andrienko, Yu., Shulga, V., Klekociuk, A., Rapoport, Yu., & Han, W. (2022b). Rossby waves in total ozone over the Arctic in 2000–2021. *Remote Sensing*, 14(9), 2192. <https://doi.org/10.3390/rs14092192>

Received: 15 December 2022

Accepted: 2 February 2023

**Ю. Ши¹, О. Євтушевський², Г. Мілінєвський^{1, 2, 3, *}, А. Грицай²,
А. Клекочук^{4, 5}, О. Іваніга^{2, 3}, Ю. Андрієнко²**

¹ Міжнародний центр науки майбутнього, Коледж фізики, Цзилінський університет,
м. Чанчунь, 130012, Китай

² Київський національний університет імені Тараса Шевченка,
м. Київ, 01601, Україна

³ Державна установа Національний антарктичний науковий центр МОН України,
м. Київ, 01601, Україна

⁴ Австралійський антарктичний департамент,
м. Кінгстон, 7050, Австралія

⁵ Університет Аделаїди, м. Аделаїда, 50005, Австралія

* Автор для кореспонденції: gennadi.milnevsky@knu.ua

Методи обробки та аналізу даних для дослідження стратосферного озону та планетарних хвиль

Реферат. Ми пропонуємо огляд методів аналізу характеристик планетарних хвиль та джерел даних, використаних в рамках спільніх досліджень нашою міжнародною командою. Описано вибрані наземні та супутникові інструменти для вимірювань озону в атмосфері та охарактеризовано можливості реаналізів атмосферних та, зокрема, озонових даних. Показані приклади даних та інструментів для аналізу. Представлена методика спектрального аналізу планетарних хвиль в умовах динамічних змін під час раптових стратосферних потеплінь. Розглянуто короткий опис основних результатів аналізу даних та використання комбінованих методів. Виявлено довготривале зміщення зонального мінімуму озону над Антарктикою на схід у весняні місяці; визначено просторові та часові характеристики віддалених зв'язків між тропічним тепловим джерелом атмосферних збурень та відгуком на них у західній частині антарктичної стратосфери; створено прогнозний індекс для можливого аномального розвитку озонової діри у весняні місяці; охарактеризовано зміни в зональній асиметрії арктичної стратопаузи; визначено особливості річного циклу озону при розгляді зональної асиметрії в його розподілі.

Ключові слова: MERRA-2, візуалізація, джерело даних, метод, озон, реаналіз